Heliyon

Received:
22 April 2016
Revised:
10 July 2016
Accepted:
16 September 2016

Heliyon 2 (2016) e00166

Gamma-tubulin coordinates nuclear envelope assembly around chromatin

Catalina Ana Rosselló, Lisa Lindström, Johan Glindre, Greta Eklund, Maria Alvarado-Kristensson *

Division of Molecular Pathology, Department of Translational Medicine, Lund University, Skåne University Hospital, Malmö, 20502. Sweden

* Corresponding author at: Maria Alvarado-Kristensson, Molecular Pathology, Lund University, SUS-MAS, 59 Jan Waldenströms Street, Floor 2, SE-205 02 Malmö, Sweden.
E-mail address: maria.alvarado-kristensson@med.lu.se (M. Alvarado-Kristensson).

Abstract

The cytosolic role of γ-tubulin as a microtubule organizer has been studied thoroughly, but its nuclear function is poorly understood. Here, we show that γ-tubulin is located throughout the chromatin of demembranated *Xenopus laevis* sperm and, as the nucleus is formed, γ-tubulin recruits lamin B3 and nuclear membranes. Immunodepletion of γ-tubulin impairs *X. laevis* assembly of both the lamina and the nuclear membrane. During nuclear formation in mammalian cell lines, γ-tubulin establishes a cellular protein boundary around chromatin that coordinates nuclear assembly of the daughter nuclei. Furthermore, expression of a γ-tubulin mutant that lacks the DNA-binding domain forms chromatin-empty nuclear like structures and demonstrate that a constant interplay between the chromatin-associated and the cytosolic pools of γ-tubulin is required and, when the balance between pools is impaired, aberrant nuclei are formed. We therefore propose that the nuclear protein meshwork formed by γ-tubulin around chromatin coordinates nuclear formation in eukaryotic cells.

Keywords: Biological sciences, Cell biology

http://dx.doi.org/10.1016/j.heliyon.2016.e00166

1. Introduction

The chain of events that leads to the formation of two identical daughter cells in cell division is highly regulated, with synchronization of cytosolic and nuclear events. Preservation of cellular homeostasis and genomic integrity requires the coordinated modification of cell components during cell division. One such component is the nuclear envelope, which separates the chromosomes from cytoplasmic structures such as the centrosomes that nucleate spindle microtubules. At the onset of mitosis the nuclear envelope disassembles to allow the mitotic spindle to segregate the condensed chromosomes between daughter cells (Collas, 1999; Peter et al., 1990) and reassembles at anaphase/telophase (Thompson et al., 1997). The nuclear lamina is a structural component of the inner surface of the nuclear envelope that provides support for chromatin domains and nuclear envelope proteins (Dechat et al., 2010) and in humans contains three major structurally related proteins named lamin A, B and C (Dechat et al., 2010). At the onset of mitosis, disperse lamin B remains associated with both the nuclear envelope membrane fragments and the mitotic spindle in the cytoplasm (Tsai et al., 2006). However, the mechanism by which nuclear assembly ensures the formation of two diploid daughter nuclei at the end of mitosis is poorly understood.

γ-Tubulin is a cytosolic protein that regulates α- and β-tubulin nucleation to a growing microtubule (Kollman et al., 2011). We and others have shown that nuclear γ-tubulin associates with Rad51, C53, GCP2, GCP3 and E2F1 (Draberova et al., 2015; Ehlen et al., 2012; Hoog et al., 2011; Horejsi et al., 2012; Lesca et al., 2005) and inhibition of the nuclear activity of γ-tubulin does not interfere with microtubule dynamics (Lindstrom et al., 2015). During the cell cycle, γ-tubulin has various functions, regulating centrosomal duplication and mitotic spindle formation and moderating transcriptional activities of E2Fs during S-phase (Hoog et al., 2011).

Although previous work has highlighted the role of microtubules and of the γ-tubulin complex protein 3-interacting proteins in shaping the nuclear envelope (Batzenschlager et al., 2013; Xue et al., 2013), it is not known whether nuclear formation and nuclear γ-tubulin are functionally linked. In the present study, we show, using both *Xenopus laevis'* extracts (Lohka and Masui, 1983) and mammalian cell lines, that γ-tubulin forms a cellular meshwork around chromatin and has two main roles during nuclear assembly. First, γ-tubulin builds up a nuclear protein boundary that connects the cytoplasm and the nuclear compartment together, and, second, γ-tubulin coordinates nuclear formation.

http://dx.doi.org/10.1016/j.heliyon.2016.e00166

2. Results

2.1. Chromatin-associated γ-tubulin is necessary for nuclear assembly

In cell lines, *TUBULIN*-shRNA expression only partially reduces the γ-tubulin protein levels (Eklund et al., 2014; Hoog et al., 2011), making depletion experiments difficult to interpret. γ-Tubulin is highly conserved among species; at the protein level human and *X. laevis* γ-tubulin-1 are 98% homologous (Fig. 1A). For this reason, *X. laevis* egg extracts have extensively been used to study the role of γ-tubulin in microtubule nucleation (Felix et al., 1994).

Analysis of demembranated *X. laevis* sperm showed that as histone 3, γ-tubulin localized throughout the DNA (Fig. 1B), whereas α-tubulin and γ-tubulin ring

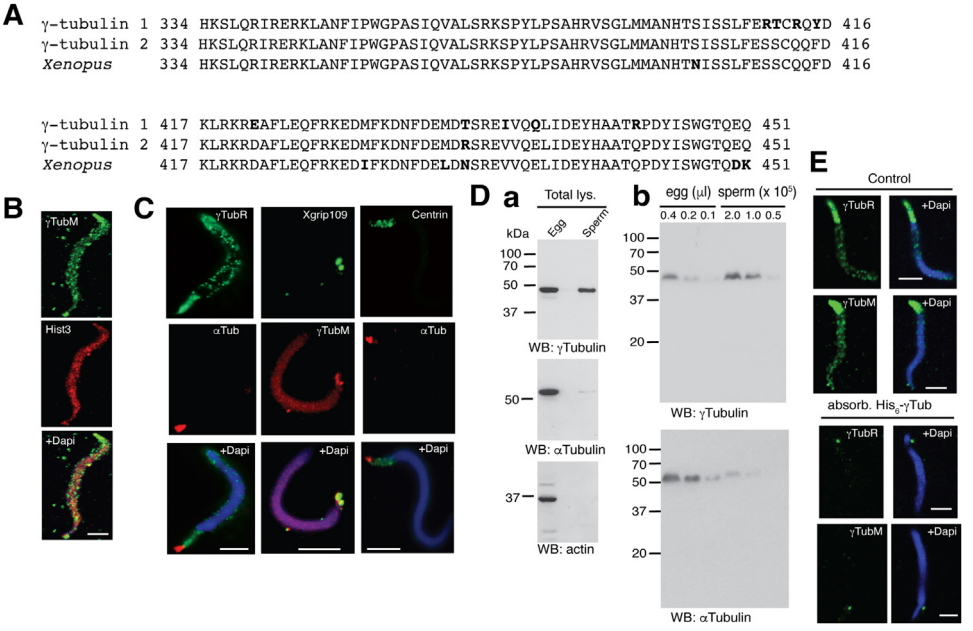

Fig. 1. Demembranated sperm contains γ-tubulin. (A) Sequence alignment of the variable region of human γ-tubulin 1 and γ-tubulin 2 and *Xenopus laevis* γ-tubulin, showing residues 334–451 of the C terminal region. Bold letters indicate differences. (B, C) The localization of γ-tubulin, histone 3, γ-tubulin ring complex (Xgrip109) and centrosome (centrin and αTub) were immunofluorescence stained in demembranated sperm ($n = 5$) with an anti-γ-tubulin antibody that was produced either in rabbit (γ-TubR; T3320) or mouse (γ-TubM; ab27074). (Da) Total lysates of egg extract and demembranated sperm were analyzed by western blotting with the indicated antibodies ($n = 3$; T3320). An actin and α-tubulin loading controls are shown. (Db) The indicated amount of egg extract (egg) and demembranated sperm (sperm) was analyzed by western blotting with the indicated antibodies ($n = 6$; T3320). An α-tubulin loading control is shown. (E) The anti-γ-tubulin antibody produced in rabbit or mouse (T3320 and ab27074) were preincubatd for 2 h with Ni^{2+} affinity resin (control) or with Ni^{2+} affinity resin associated with His_6-tagged γ-tubulin (absorb. His_6-γ-Tub) before immunofluorescence staining the sperm. In (B, C, E) γ-tubulin is shown as green and histone 3 as red and nuclei as blue (DAPI). In (C) Xgrip109 and γTub are shown as green and red, respectively. Scale bars, 10 μm.

http://dx.doi.org/10.1016/j.heliyon.2016.e00166

complex protein, Xgrip109 (Martin et al., 1998), were found in one end of the sperm (Fig. 1C). Simultaneous staining of α-tubulin and centrin showed the centrosomal localization of αβ-tubulin dimers (Fig. 1C) and explained the presence of αβ-tubulin in the sperm (Fig. 1D). Notably, the observed constitutive location of endogenous γ-tubulin to the chromatin of sperm was reduced upon preincubation of the anti-γ-tubulin antibody (T3320 or ab27074) with Ni^{2+} affinity resin associated His_6-tagged γ-tubulin before immunofluorescence staining the sperm (Fig. 1E), demonstrating the specificity of the immunofluorescence staining. Western blot analysis of γ-tubulin confirmed that both egg extracts and sperm contained γ-tubulin, although, the γ-tubulin to α-tubulin expression ratio was approximately nine to seventeen fold higher in the sperm (13.0 ± 8.2; $n = 7$) (Fig. 1D).

To exclude an involvement of αβ-tubulin in the initial events leading to nuclear formation, we prepared the sperm in the presence of colcemid and removed αβ-tubulin debris by a glycerol cushion (Fig. 2A) (Felix et al., 1994). This treatment reduced the amount of αβ-tubulin and centrin associated to the sperm (Fig. 2A). Addition of egg extracts to the colcemid pretreated sperm triggered nuclear formation (Fig. 2B) (Lohka and Masui, 1983). Furthermore, 100% of the formed nuclei excluded TRITC-labeled 155-kDa dextran (99.7 ± 0.6; $n = 3$) and assembled nuclear pore complexes, confirming the integrity of the nuclei (Fig. 2C).

During nuclear assembly, the sperm undergo four distinct morphological stages before forming a nuclear γ-tubulin boundary (Fig. 2B). In stage 1, the sperm is condensed and in stage 2, decondensed. An almost formed nucleus is observed in stage 3 and is larger during stage 4. Chromatin-associated γ-tubulin was localized throughout the sperm chromatin in stage 1 to 3 and enriched at the nuclear envelope (NE) in stage 4 (Fig. 2B), but was not in complex with Xgrip109 (Fig. 2D).

To find functional links between αβ-tubulin and chromatin-associated γ-tubulin, we studied the location of α-tubulin during nuclear formation and found that γ- and α-tubulin coincided in centrosomes (Fig. 2E) (Xue et al., 2013). To investigate the role of αβ-tubulin, we performed nuclear assembly reactions in the presence of various concentrations of colcemid and assayed its effect on the formation of endogenous microtubules. Supplementation with 100 ng/ml colcemid depolymerized microtubules (Fig. 2F), but neither impaired nuclear formation, nor affected the location of γ-tubulin, suggesting that γ-tubulin has microtubule-independent functions during nuclear assembly (Fig. 2E, F).

Immunodepletion of γ-tubulin from egg extracts reduced the amount of γ-tubulin by $54 \pm 6\%$ (Fig. 3A; $n = 6$) and caused a trend towards decrease nuclear formation (Fig. 3B). To further improve the degree of γ-tubulin immunodepletion in the sperm (Fig. 1B-E; stage 1), we removed chromatin-bound proteins with

http://dx.doi.org/10.1016/j.heliyon.2016.e00166

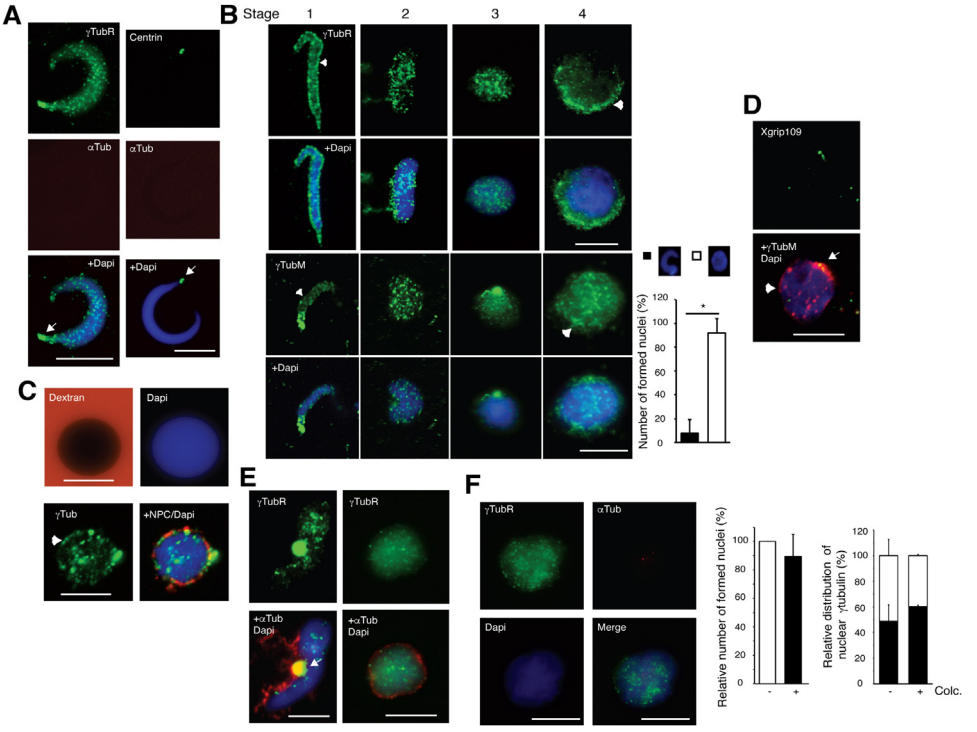

Fig. 2. γ-Tubulin and α-tubulin are differently distributed. (A) γ-Tubulin (T5192), α-tubulin and centrin were immunofluorescence stained in demembranated sperm that were isolated in the presence of colcemid and pelleted onto a cushion containing SuNaSp and glycerol before the immunostaining (n = 5). (B) To study morphological changes, demembranated sperm were incubated with egg extracts during 0 min (stage 1, condensed sperm) or 60 min before fixation (stage 2, decondensed; stage 3, small almost-formed nucleus; and stage 4, nucleus with a γ-tubulin boundary). Localization of γ-tubulin was examined by immunofluorescence staining with a rabbit and a mouse produced anti-γ-tubulin antibody, as indicated. Graph shows the mean percentage of formed nuclei (open bar; stage 3 and 4; ± s.d., n = 3; * $p < 0.05$). (C) To test the integrity of formed nuclei, nuclear assembly reactions were incubated with TRITC-labeled dextran. Alternatively, nuclear pore complexes (NPC) were immunofluorescence stained (n = 3). (D-F) Demembranated sperm prepared as in Fig. 1B (D, E) or as in A (F) were incubated in the presence of egg extracts for 60 min before fixation in the absence (D, E) or presence (F) of colcemid. The localization of Xgrip109, microtubules (αTub), centrosomes (γTub and αTub) and γ-tubulin were examined by immunofluorescence staining (n = 3). (F) From left to right, first graph shows the mean percentage of formed nuclei in the presence of colcemid (black bar) relative to a non-treated control egg extracts and sperm (open bar). Second graph displays mean percentage of formed nuclei with γ-tubulin localized throughout the nuclei (black bar) or marginalized to the nuclear envelope (open bar) (± s.d., n = 3). In (A-C, E, F) γ-tubulin and centrin are shown as green, α-tubulin and NPC as red and nuclei as blue (DAPI). In (D) Xgrip109 and γTub are shown as green and red, respectively. Arrows and arrowheads indicate the location of centrosomes and the γ-tubulin nuclear boundary, respectively. Scale bars, 10 μm.

proteinase K (Ksperm; Fig. 3C) and found that only depletion of γ-tubulin in both sperm and egg extracts significantly impaired nuclear formation (Fig. 3A-D). Furthermore, supplementation of the egg extracts with recombinant γ-tubulin partially re-established nuclear formation, but it was not as efficient as when added to the sperm (Fig. 4A). Indeed, supplementation of Ksperm with recombinant

http://dx.doi.org/10.1016/j.heliyon.2016.e00166

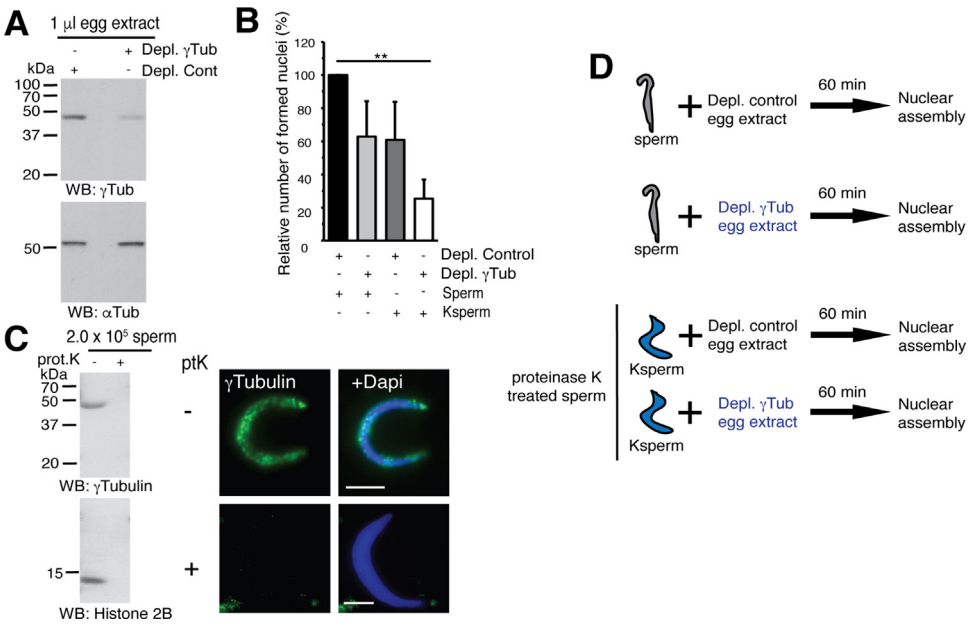

Fig. 3. Nuclear γ-tubulin is necessary for nuclear assembly. (A) Nuclear assembly was performed as in Fig. 2B. Egg extracts (egg extr.) were immunodepleted in the presence (Depl. γTub) or absence (Depl. Cont.) of an anti-γ-tubulin antibody by immunoprecipitation and protein levels of γ-tubulin and α-tubulin were analyzed by WB ($n = 6$). (B) Graph shows the mean percentage of formed nuclei in stage 3 and 4 relative to a control (black bar) in nuclear assembly reactions that were performed under the conditions described in D (± s.d., $n = 3$, ** $p < 0.01$). (C) Proteins associated with the demembranated sperm were degraded with proteinase K (ptK; Ksperm), as indicated and remaining protein levels of γ-tubulin and histone 2B were analyzed by western blotting (WB). The localization of γ-tubulin and chromatin in sperm were assayed by immunofluorescence with an anti-γ-tubulin antibody (green; ab27074) and by DAPI staining (blue; $n = 3$). (D) Schematic representation describing the conditions used during nuclear assembly assays. The figure shows representative images from at least ten experiments. Scale bars, 10 µm.

γ-tubulin-1 or the transcription factor E2F1 mutant, $E2F1^{\Delta 194-426}$ (Hoog et al., 2011) proved that only γ-tubulin re-established nuclear formation (Fig. 4A). These data imply that γ-tubulin is necessary for nuclear assembly.

2.2. Nuclear membranes and lamin B3 are recruited to γ-tubulin enriched regions

To describe the exact function of γ-tubulin during nuclear assembly, we monitored formation of the lamina and of the NE by immunostaining lamin B3, the most abundant lamin present in *X. laevis* eggs (Lourim et al., 1996), and by staining membranes with the lipophilic dye Nile Red (Cox and Leno, 1990; Leno and Laskey, 1991; Lu et al., 1997), as well as analyzing γ-tubulin localization. Demembranated sperm contained a boundary of γ-tubulin but lacked an intact lamina and NE (Fig. 4B, C; 0 min). Addition of egg extract recruited lamin B3 and nuclear membranes (NM) to γ-tubulin enriched areas (Fig. 4B, C; 90 min), which

http://dx.doi.org/10.1016/j.heliyon.2016.e00166

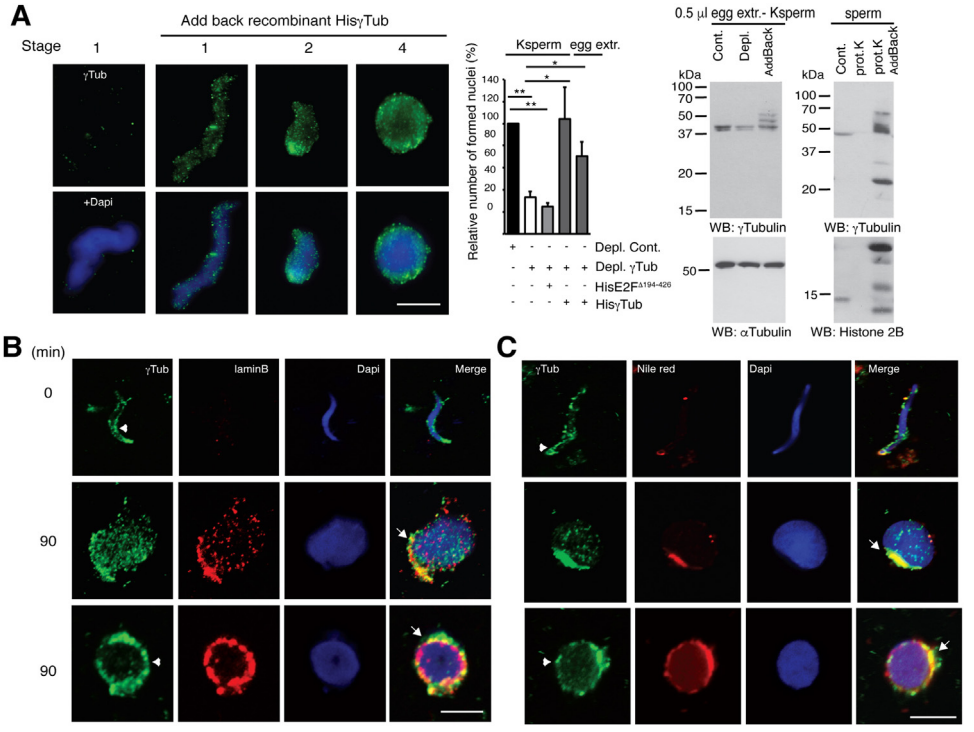

Fig. 4. Recombinant γ-tubulin restores nuclear assembly. (A) Nuclear assembly was performed as in Fig. 3. Bacterially produced His_6–γ-tubulin (HisγTub) or His_6–$E2F1^{\Delta 194-426}$ ($HisE2F^{\Delta 194-426}$) was added back (addback) to Ksperm or to immunodepleted egg extract (egg extr.) and the effects of His_6–γ-tubulin on nuclear assembly were examined. The protein levels of γ-tubulin in extracts (egg extr.-Ksperm) or sperm were analyzed by WB as indicated. An α-tubulin (αTub) loading control is shown (n = 3-6). Graphs show mean percentage of formed nuclei in stage 3 and 4 relative to a control (black bar) from nuclear assembly reactions that consisted of immunodepleted egg extracts and sperm or Ksperm, in which an anti-γ-tubulin antibody (open bar; T3320) or an anti-γ-tubulin antibody that after immunodepletion, either His_6–γ-tubulin or His_6–$E2F1^{\Delta 194-426}$ was added to Ksperm or to depleted egg extract (grey bar; ± s.d., n = 3-6 for each graph; * $p < 0.05$, ** $p < 0.01$). (B, C) Confocal images of the morphological changes of nuclei in stage 1, 3 and 4 from a nuclear assembly of egg extracts and sperm treated as in Fig. 3 but incubated for 90 min before fixation to increase the number of nuclei in stage 4. Arrowheads show γ-tubulin boundaries around sperm and nuclei. Arrows show γ-tubulin–lamin B3 enriched areas. In (A-C) γ-tubulin (γTub; green;) and lamin B3 (laminB; red) are shown as immunofluorescence staining with an anti-γ-tubulin and an anti-lamin B3 antibody. Nuclear membranes and nuclei were detected with Nile red (red) and DAPI (blue), respectively. The figure shows representative images from at least ten experiments. Scale bars, 10 µm.

suggest that lamin B3 and NM may be recruited to the NE in a γ-tubulin dependent manner.

2.3. The C-terminal region of γ-tubulin regulates nuclear formation

To elucidate the role of γ-tubulin, we monitored nuclear formation in the absence of γ-tubulin and found that the chromatin was neither able to form lamina or to

http://dx.doi.org/10.1016/j.heliyon.2016.e00166

recruit NM (Fig. 5A). Addition of human γ-tubulin to the Ksperm enabled the formation of the NE and of the lamina meshwork again (Fig. 5A).

To identify the γ-tubulin-domain important in nuclear formation, we tested various γ-tubulin mutants (Fig. 5B). Bacterially produced His_6-γtubulin and His_6-C-γtub$^{334–452}$, but not His_6-N-γtub$^{1–333}$ bound to chromatin during nuclear formation (Fig. 5B) and abolished the inhibiting effect of γ-tubulin depletion (Fig. 5A). This observation proves that both exogenous γ-tubulin and its C-terminal domain bind

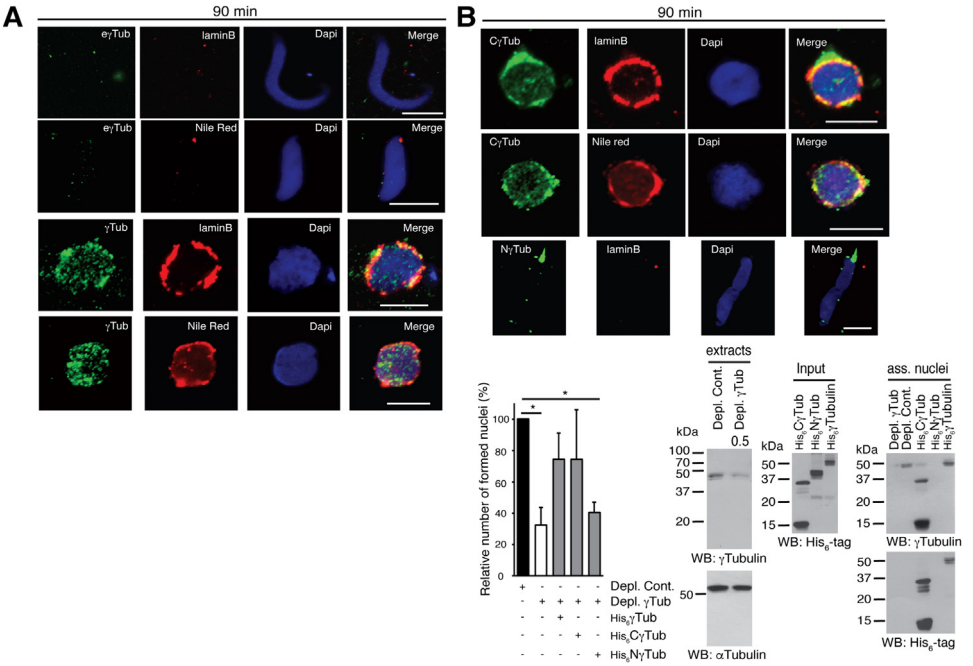

Fig. 5. Nuclear-γ-tubulin promotes the formation of the nuclear envelope and the lamina meshwork. (A, B) Ksperm were incubated in the presence of γ-tubulin immunodepleted egg extracts (Depl.) during 90 min before fixation or before spun down through a sucrose cushion for analysis by WB (ass. nuclei). Representative confocal fluorescence images of morphological changes of nuclei in stage 1 or 4 showing the location of endogenous γ-tubulin (eγTub, green) or bacterially produced His_6–γ-tubulin (γTub, green), His_6–C-γtub$^{334–452}$ (CγTub, green) or His_6–N-γtub$^{1–333}$ (NγTub, green) of nuclei in stage 1 or 4. Localization of lamin B3 (lamin B; red) were examined by immunofluorescence staining with an anti-lamin B3 antibody and nuclear membranes and nuclei were detected with Nile red (red) and DAPI (blue), respectively. Localization of γ-tubulin, His_6–γ-tubulin, His_6–C-γtub$^{334–452}$ and His_6–N-γtub$^{1–333}$ were immunofluorescence stained with either T3320 (eγTub, γTub, CγTub) or T5192 (NγTub). The figure shows representative images from at least five experiments. Scale bars, 10 μm. (B) Graph shows the mean percentage of assembled nuclei in stage 3 and 4 versus a control (black bar), with an anti-γ-tubulin antibody (open and grey bars) and with each form of His_6–γ-tubulin (grey bars) added back ($n = 3$; * $p < 0.05$), as indicated. The amount of protein added back (input), the γ-tubulin level present in the extracts and the association of His_6–γ-tubulin, His_6–C-γtub$^{334–452}$ and His_6–N-γtub$^{1–333}$ with assembled nuclei were analyzed by WB with the indicated antibodies. Numbers on WBs indicate the level of depletion of γ-tubulin in the extracts relative to control. To adjust for differences in protein loading, the protein concentration of γ-tubulin was determined by its ratio with α-tubulin for each sample. The protein ratio in control extracts was set to 1.

http://dx.doi.org/10.1016/j.heliyon.2016.e00166

back to chromatin. In addition, it also demonstrates that the C-terminal domain is the necessary domain for nuclear and lamina assembly and notably, this domain contains γ-tubulin's DNA binding motif (Fig. 1A) (Hoog et al., 2011).

2.4. γ-Tubulin recruitment of nuclear membranes is independent of lamina formation

Interference with the function of lamin B3 affects the size of the formed nuclei (Lourim et al., 1996). To test whether the defects in nuclear assembly observed following γ-tubulin depletion are due to an impaired lamina formation or lamin B3 recruitment to chromatin, we added recombinant lamin B3 to Ksperm (Fig. 6A). In the absence of chromatin-bound γ-tubulin, lamin B3 did not associate with Ksperm and, consequently, addition of recombinant lamin B3 was not sufficient to trigger neither lamina nor nuclear formation (Fig. 6A), suggesting that lamin B3 needs to be recruited to chromatin by γ-tubulin.

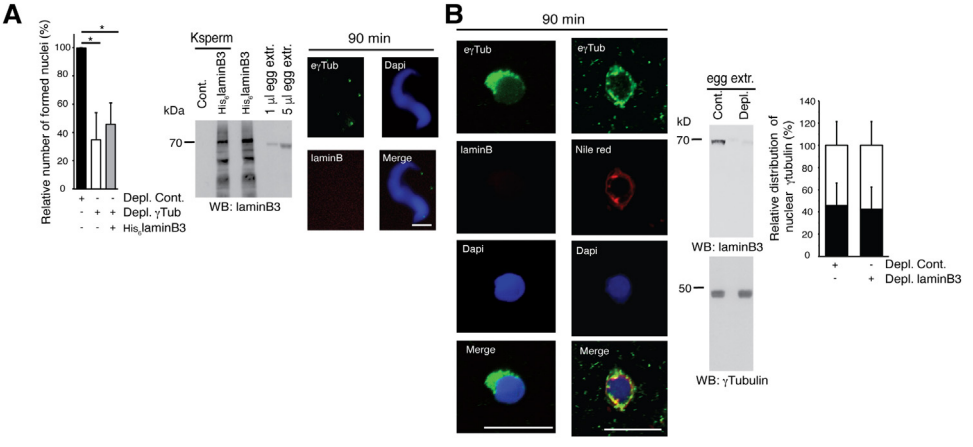

Fig. 6. γ-Tubulin promotes the formation of the nuclear envelope in the absence of lamin B3. (A) His_6–lamin B3 (laminB3) was added back to Ksperm (Cont.; Ksperm without laminB3) and γ-tubulin immunodepleted egg extract (Depl.) and nuclear assembly was performed as in Fig. 5. Graph shows the mean percentage of formed nuclei in stage 3 and 4 in immunodepleted egg extracts and sperm (Depl. γTub) versus a control (black bar; Depl. Cont.), with addition of His_6–lamin B3 (grey bar) to the γ-tubulin depleted extracts (± s.d., $n = 3$; * $p < 0.05$), as indicated. The western blot shows the amount of His_6–lamin B3 added to sperm. To relate the amount of His_6–lamin B3 to the amount present in extracts, 1 µl and 5 µl of egg extracts were loaded. Representative confocal fluorescence images of morphological changes of nuclei show the location of endogenous γ-tubulin (eγTub, green) or lamin B (red). (B) Representative confocal fluorescence images of morphological changes of nuclei in nuclear assembly reactions that were triggered by addition of lamin B3 immunodepleted egg extracts to sperm and incubated 90 min before fixation. The protein levels of lamin B3 in extracts were analyzed by WB. The graph shows the mean percentage of formed nuclei with γ-tubulin localized throughout the nuclei (black bar) or marginalized to the nuclear envelope (open bar) (± s.d., $n = 3$). (A, B) Localization of γ-tubulin (eγTub; green), His_6–lamin B3 (lamin B; red) and lamin B3 (lamin B; red) were examined by immunofluorescence staining with the indicated antibody and nuclear membranes and nuclei were detected with Nile red (red) and DAPI (blue), respectively. The figure shows representative images from at least five experiments. Scale bars, 10 µm.

http://dx.doi.org/10.1016/j.heliyon.2016.e00166

Finally, to demonstrate that the role of γ-tubulin in nuclear formation is independent of the formation of the lamina, we immunodepleted lamin B3 from egg extracts and studied the location of γ-tubulin and NM. Indeed, the lack of lamin B3 neither affected the location of γ-tubulin or the recruitment of NM (Fig. 6B). These data prove that recruitment of NM by the nuclear γ-tubulin boundary is independent from formation of the lamina meshwork.

2.5. Endogenous γ-tubulin forms a cellular protein meshwork

In an asynchronous cell population, approximately 26% of the total amount of endogenous γ-tubulin is associated with chromatin in U2OS and NIH3T3 cells (Eklund et al., 2014; Hoog et al., 2011). To understand the interconnection between the cytosolic and the nuclear γ-tubulin pools, we performed confocal microscopy and superresolution microscopy of the top plane (Fig. 7A) and mid plane (Fig. 7B and Fig. 8) of fixed U2OS cells and of living U2OS cells that stably co-expressed *γTUBULIN* shRNA (*γTUBULIN*sh-U2OS) and human GFP-tagged sh-resistant γ-tubulin (*γTUBULIN*sh-U2OS-GFP-γ-tubulin$_{resist}$; Fig. 9A, B) and transiently expressed mCherry-tagged lamin B (mCherry-lamin B1; Fig. 9B). The *γTUBULIN* shRNA reduced the expression of endogenous γ-tubulin by approximately 50% (53 ± 6%, $n = 3$; Fig. 9A) and we compensated for this reduction by stably co-expressing GFP-γ-tubulin$_{resist}$ (Fig. 9A, B).

Confocal microscopy of the top plane (Fig. 7A) and mid plane (Fig. 7B and Fig. 8) of fixed U2OS cells and Z-stack images of whole living *γTUBULIN*sh-U2OS-GFP-

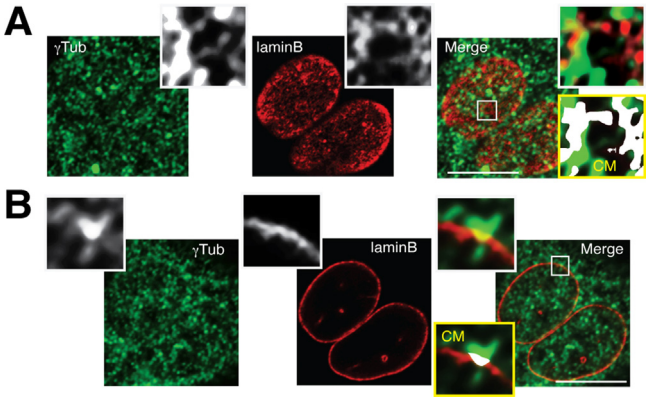

Fig. 7. Endogenous γ-tubulin bridges connect both the nuclear and the cytosolic γ-tubulin pools across the nuclear envelope. (A, B) Localization of endogenous γ-tubulin with an anti-γ-tubulin (T3320; green), lamina with an anti-lamin B (laminB; red) antibody and nuclei with DAPI (blue) were examined in U2OS cells in interphase. Confocal images are the mid planes of the γ-tubulin boundary at the nuclear membrane (A) or of the nuclear compartment (B) of a U2OS cell. White and yellow boxes show the magnified areas and colocalization pixel-map (CM) of the red and green channels of the magnified areas displayed in the inset, respectively. White areas in CM denote colocalized pixels between channels. The figure shows representative images from at least five experiments. Scale bars, 10 μm.

http://dx.doi.org/10.1016/j.heliyon.2016.e00166

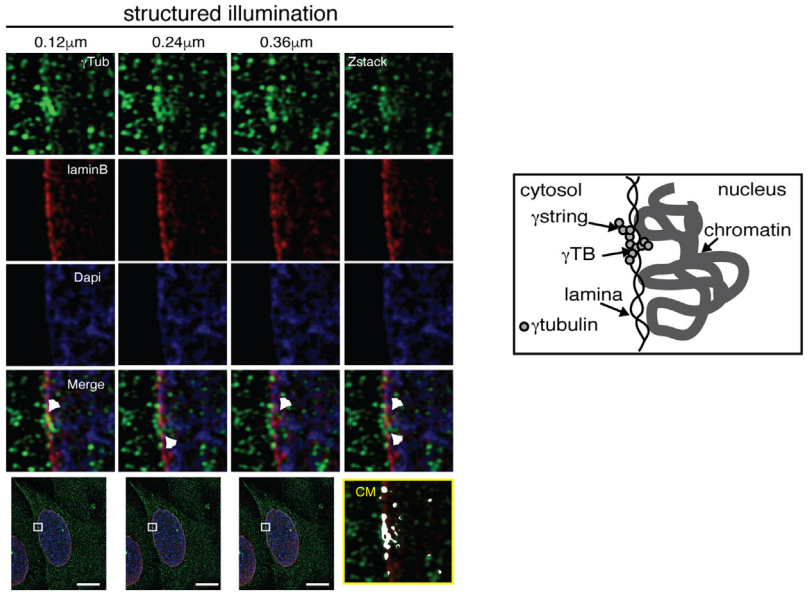

Fig. 8. γ-strings are intertwined with the lamina meshwork. Localization of endogenous γ-tubulin with an anti-γ-tubulin (T6557; green), lamina with an anti-lamin B (laminB; red) antibody and nuclei with DAPI (blue) were examined in U2OS cells in interphase. Structured illumination images are the mid planes of the nuclear compartment of a U2OS cell. Z-stack images were collected at 0.12 μm intervals. Z-stack shows average intensity projection of the displayed three Z-stack images. The white box shows the magnified areas. Arrowheads show protein bridges of γ-tubulin. The yellow box shows colocalization pixel-map (CM) of the red and green channels. White areas in CM denote colocalized pixels between channels. The figure shows representative images from four experiments. Scale bars, 10 μm. Right panel, γ-tubulin forms strings (γstrings) that act as protein bridges (γTB) between the cytosolic and the nuclear compartment. In their way into the nucleus, a γ-string goes through the nuclear lamina.

γ-tubulin$_{resist}$ cells (Fig. 9B) showed that on the NE, endogenous and recombinant γ-tubulin formed strings and together with lamin B formed an interconnected protein meshwork on both the lower (Fig. 9B; 0.34–1.36 μm) and on the higher nuclear surface (Fig. 7A and Fig. 9B; 3.06–3.74 μm). On the NE, endogenous γ-tubulin strings looked similar to lamin B fibers (Fig. 7A). However, the lamin B1 meshwork became non-detectable in the nuclear compartment (Fig. 9B; 0.68–3.06 μm). In contrast, the γ-tubulin strings were detected throughout the nucleus (Fig. 9B; 0.34–3.74 μm) and established γ-tubulin protein bridges between the cytoplasm and the nuclear compartment (Fig. 7B, Fig. 8 and Fig. 9B).

To exclude the possibility that fixation of the cells caused formation of γ-tubulin strings, we studied the location of the protein centrin. In comparison with γ-tubulin, immunofluorescence staining with an anti-centrin antibody showed that centrin formed no cellular strings (Fig. 9C, D). Accordingly, the localization of both the nuclear GFP-tagged human RNA-binding protein 3 (GFP-RBM3) and of the cytosolic GFP-tagged ser/thr kinase SADB-long (mSADB, hSAD1/BRSK1;

http://dx.doi.org/10.1016/j.heliyon.2016.e00166

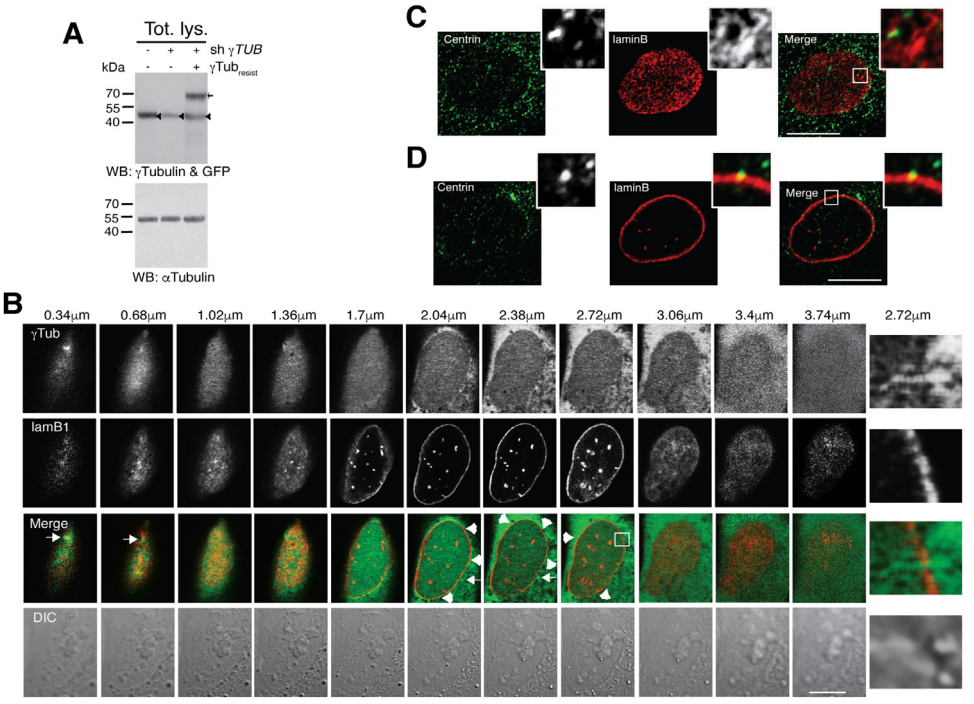

Fig. 9. γ-Tubulin forms a cellular meshwork. (A) Total lysate from U2OS, U2OS cells stably expressing *γTUBULIN* shRNA (sh*γTUB*) and U2OS cells stably expressing *γTUBULIN* shRNA and GFP-γ-tubulin$_{resist}$ (γTub$_{resist}$, $n = 3$) were analyzed by WB for the expression of endogenous γ-tubulin (arrowhead) and GFP-γ-tubulin$_{resist}$ (arrow) with a mixture of an anti-γ-tubulin (T6557) and an anti-GFP (sc-8334) antibody. An α-tubulin loading control is shown. (B) Differential interference contrast (DIC)/fluorescence images of a Z-stack of U2OS cells stably expressing *γTUBULIN* shRNA and GFP-γ-tubulin$_{resist}$ (γ-TubGFP; green) and transiently expressing mCherry-tagged lamin B (red). Images were collected at 0.34 μm intervals. Z-stack images taken in the intervals 0.34–1.36 μm and 3.06–3.74 μm show the lower and the higher γ-string meshwork formed on the nuclear envelope, respectively. Z-stack images in the interval 1.7–2.72 μm show the γ-string meshwork in the nuclear compartment. Arrows and arrowheads show the centrosomes and γ-tubulin bridges, respectively. The magnified area (white border) shows a γ-tubulin bridge (right panels). The figure shows representative images from at least eight experiments. (C, D) Localization of endogenous centrin with an anti-centrin (green) and lamina with an anti-lamin B (laminB; red) antibody were examined in U2OS cells in interphase. Confocal images are the mid planes of the nuclear membrane (C) or of the nuclear compartment (D) of U2OS cells. (B-D) Scale bars, 10 μm.

GFP-SADB$_L$) differed from γ-tubulin in the NE. Z-stack images of whole living U2OS cells transiently expressing either GFP-RBM3 or GFP-SADB$_L$ showed that neither GFP-RBM3 nor GFP-SADB$_L$ were found to continue cross the NE (0.34–0.68 μm and 2.72–3.74 μm RBM3 and 0.34–0.68 μm and 3.06–3.74 μm SADB$_L$; Fig. 7A, B, Fig. 9B and Fig. 10A, B). Altogether, these data confirm that γ-tubulin forms a meshwork that connects the chromatin to the cytoplasm.

http://dx.doi.org/10.1016/j.heliyon.2016.e00166

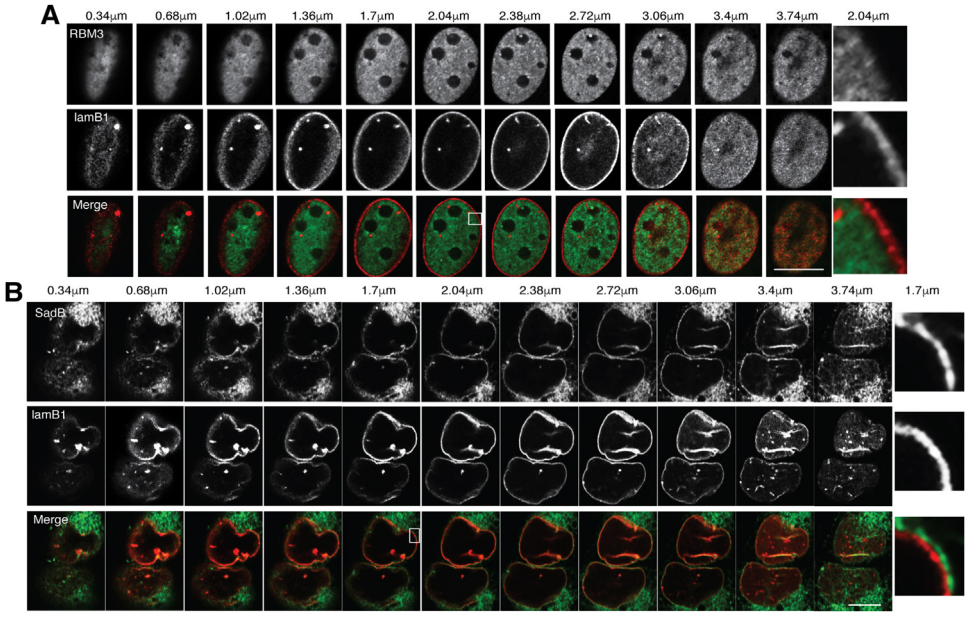

Fig. 10. Neither RBM3 nor $SadB_L$ form a cellular meshwork. (A, B) Confocal images of a Z-stack of U2OS cells transiently expressing either GFP-RBM3 (RBM3; A) or GFP-$SadB_L$ (SadB; B), and transiently expressing mCherry-tagged lamin B (laminB1). Images were collected at 0.34 μm intervals. (A) Z-stack images taken in the intervals 0.34–0.68 μm and 2.72–3.74 μm show the nuclear envelope and in the interval 1.02–2.38 μm shows the nuclear compartment of cells expressing RBM3. (B) Z-stack images taken in the intervals 0.34–0.68 μm and 3.06–3.74 μm show the nuclear envelope and in the interval 1.02–2.72 μm shows the nuclear compartment of cells expressing SADB. (A, B) The magnified area (white border) shows the mid plane of the nuclear compartment (right panels). Scale bars, 10 μm.

2.6. The γ-tubulin meshwork consists of strings

To characterize the structure of the γ-tubulin meshwork, we performed immunoelectron microscopy of U2OS cells that were prepared with two different methods. In the first method, we high-pressure frozen U2OS cells (Fig. 11). In the second method, we tested various fixation procedures and found that short fixation (5 min) of cells with 4% paraformaldehyde preserved the γ-tubulin meshwork. With both methods, we detected strings in both cytoplasm and nucleus that went across the NE (Fig. 11A and Fig. 12A). Immunoelectron microscopy confirmed that the antibody recognized strings with a 4 to 6 nm in diameter, which from now on will be referred as γ-strings (Fig. 11A and Fig. 12A; $n = 19$). γ-Strings were attached to the plasma membrane (Fig. 11A and Fig. 12A), occurred in both the outer, the inner nuclear membrane (Fig. 11A and Fig. 12A) and in the nuclear compartment (Fig. 11A and Fig. 12A) and connected both the nuclear and the cytosolic γ-tubulin pools across the NE (Fig. 11A and Fig. 12A). By contrast, control immunostaining with an anti-α-tubulin antibody recognized cytosolic arrays of microtubules (Fig. 11B). Together these data demonstrate the existence of a NE-associated network, the γ-string meshwork.

http://dx.doi.org/10.1016/j.heliyon.2016.e00166

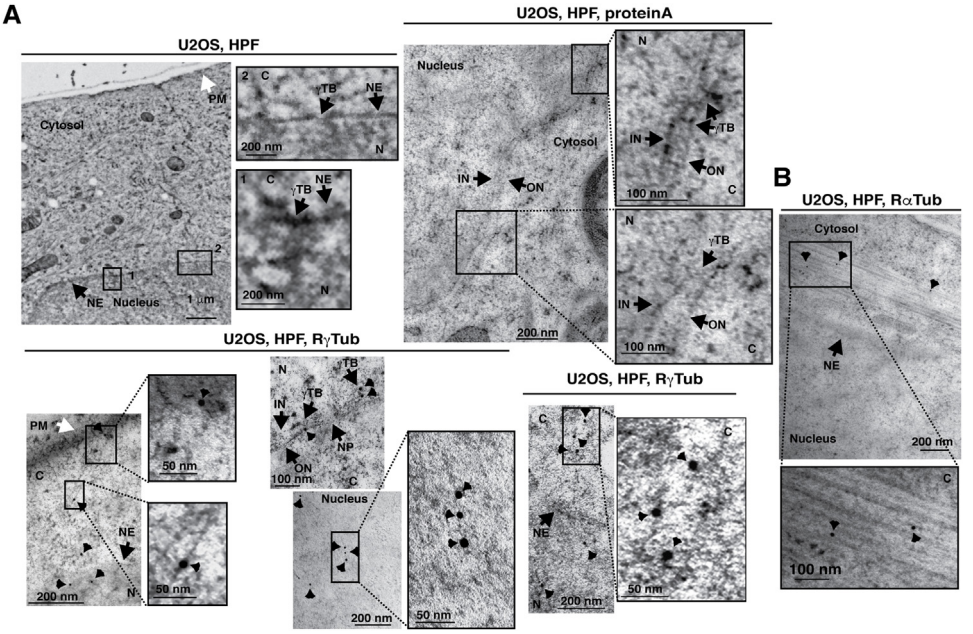

Fig. 11. The cytosolic and the nuclear pools of γ-tubulin are connected and form one protein meshwork. (A, B) Endogenous γ-tubulin detection in immunoelectron microscopy using three different conditions in high pressure frozen (HPF) U2OS cells: first, no antibody (A), second, gold conjugated protein A (A) and third, an anti-γ-tubulin antibody (T3320; A) and gold conjugated protein A (RγTub; A) or an anti-α-tubulin antibody and gold conjugated protein A (RαTub; B). Images show the plasma membrane [PM], cytosol [C], nuclear envelope [NE], inner [IN] and outer [ON] nuclear membranes and nucleus [N] and γ-tubulin bridges [γTB] of a U2OS cell. A black box shows the magnified area displayed in the inset. Black arrowheads show either immunolabeled γ-strings (RγTub) or immunolabeled microtubules (RαTub). Arrows show the indicated structure ($n = 3$).

To finally prove that the observed γ-strings are made of γ-tubulin and to study the *in vitro* effect of γ-tubulin on lamina formation, we investigated the *in vitro* ability of γ-tubulin to form strings and to assist lamina formation. Electron microscopy analysis of bacterially produced γ-tubulin showed that *in vitro* γ-tubulin formed a meshwork of strings only in the absence of GTP (Fig. 12B). Furthermore, the formed meshwork supported formation of lamin B3 protofilaments (Fig. 12B), confirming that γ-tubulin forms strings that assist initial nucleation of lamin B3 into a protofilament.

2.7. The protein levels of γ-tubulin affect the integrity of the lamina

A chromatin-associated protein meshwork that facilitates lamina formation may provide a cell with a scaffold that maintains the NE. To test this, we isolated nuclei from both U2OS, *γTUBULIN*sh-U2OS-GFP-γ-tubulin$_{resist}$ and *γTUBULIN*sh-U2OS cells (Fig. 13A-C) (Mendez and Stillman, 2000) and found that the nuclei contained a nuclear boundary of γ-strings to which microtubule components were

http://dx.doi.org/10.1016/j.heliyon.2016.e00166

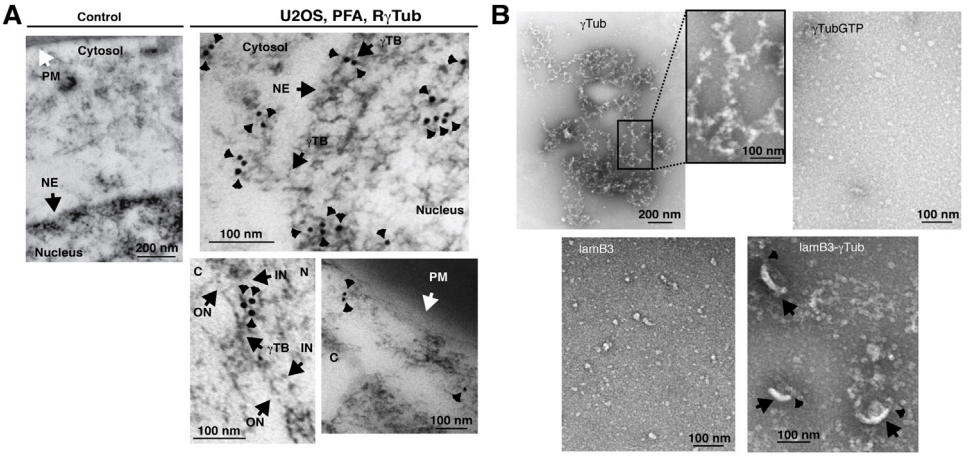

Fig. 12. The γ-tubulin meshwork supports formation of lamin B3 protofilaments. (A) Endogenous γ-tubulin detection in immunoelectron microscopy using an anti-γ-tubulin antibody or no primary antibody (control) on paraformaldehyde fixed (PFA) U2OS cells. Images show the plasma membrane [PM], cytosol [C], nuclear envelope [NE], inner [IN] and outer [ON] nuclear membranes and nucleus [N] and γ-tubulin bridges [γTB] of a U2OS cell. A black box shows the magnified area displayed in the inset. Black arrowheads show either immunolabeled γ-strings (RγTub) or immunolabeled microtubules (RαTub). Arrows show the indicated structure ($n = 3$). (B) Purified γ-tubulin and lamin B3 (lamB3) were negatively stained and imaged by electron microscopy in the absence (γ-Tub) or presence of 1 mM GTP (γ-TubGTP). The magnified area (black border) shows γ-strings and arrows and arrowheads show lamin B3 fibers and γ-strings, respectively.

associated on the cytosolic side (Fig. 13A). Isolated nuclei from cytochalasin B and colcemid treated cells (Alvarado-Kristensson et al., 2009) had no attached microtubules (Fig. 13B), but still contained a γ-string boundary intertwined with the lamina (Fig. 13C). In addition, isolated nuclei from *γTUBULIN*sh-U2OS cells showed that 86% of cells with low expression of γ-tubulin had a scattered lamin B meshwork (Fig. 13D), which imply that the γ-tubulin-nuclear boundary formed at the transition between cytosolic and chromatin-associated γ-strings may function as a supporting scaffold for the lamina.

Finally, to examine the interactions of γ-strings with the lamina, we analyzed the lamin and the tubulin content of endogenous γ-tubulin and lamin B immunoprecipitated from cytoplasmic, nuclear membrane and chromatin fractions of NIH3T3 and U2OS cells. We found that although association with the other lamina components, lamin A and C, was only observed in the chromatin fractions, γ-tubulin–lamin B complexes were immunoprecipitated from all cellular fractions (Fig. 13E; Fig. S1), suggesting a function of γ-tubulin in lamin B recruitment to the NE.

http://dx.doi.org/10.1016/j.heliyon.2016.e00166

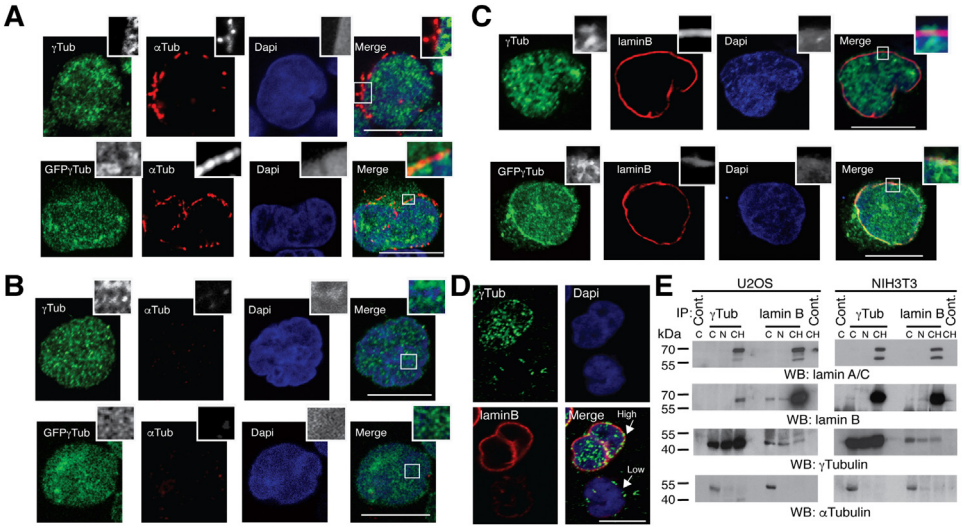

Fig. 13. γ-Tubulin forms a boundary on the cytosolic side of the nucleus and its disruption affects the integrity of the lamina. (A-D) Confocal images of isolated nuclei purified in the absence (A) or presence (B-D) of cytochalasin B and colcemid from U2OS (γTub) and stable *γTUBULIN* shRNA-GFP-γ-tubulin$_{resist}$ (GFPγTub) and *γTUBULIN* shRNA expressing cells. (A-C) White borders show the magnified areas displayed in the insets: the γ-string meshwork on the nuclear envelope (A-C), the γ-string boundary (A, B), chromatin-associated γ-strings (B) or γ-string bridges (C). In (A-D) γ-tubulin (γTub; green, T3320), α-tubulin (αTub; red) and lamin B (laminB; red) are shown as immuofluorescence staining and nuclei were detected with DAPI (blue). (D) shows the endogenous expression of lamin B and γ-tubulin in two nuclei containing either high or low γ-tubulin expression, as indicated. (A-D) Scale bars, 10 μm. (E) U2OS and NIH3T3 cells (20×10^6 cells) were biochemically divided into cytosolic [C], nuclear membrane [N], and chromatin [CH] fractions. Each fraction was subjected to immunoprecipitations (IP) with an anti-γ-tubulin (γTub; T6557), anti-lamin B or anti-GFP (Cont.) antibody, as indicated, and developed by WB with antibodies against lamin A/C, lamin B, γ-tubulin (T5192) and α-tubulin antibody ($n = 5$). (A-E) The figure shows representative images from at least five experiments. See also Fig. S1.

2.8. The γ-string boundary supports the formation of the lamina

Based on the finding of the γ-string boundary, we hypothesized that it may provide a cell with a tool to structure synchronized cytosolic and nuclear events during cell division. To visualize the interconnection between γ-strings and lamina formation during nuclear assembly, we analyzed time-lapse images of dividing *γTUBULIN*sh-U2OSGFP-γ-tubulin$_{resist}$ (with C-terminal tagged γ-tubulin; Fig. 14; movie S1), U2OS (Fig. 15A; movie S2) and *γTUBULIN*sh-U2OS cells (Fig. 15B; movie S3) that transiently co-expressed mCherrylamin B1. In metaphase, γ-tubulin was evenly distributed throughout the cell (Fig. 14, 0 min) and a γ-tubulin-boundary composed of cytosolic and chromatin-associated γ-strings around the mitotic chromosomes (Fig. 14, 0–3 min) was observed. This γ-tubulin-boundary remained in the newly formed daughter nuclei (Fig. 14, 4–12 min). In contrast, in metaphase lamin B remained non-chromatin bound (Fig. 14, 0–3 min). During early telophase the lamina became visible and grew over time

http://dx.doi.org/10.1016/j.heliyon.2016.e00166

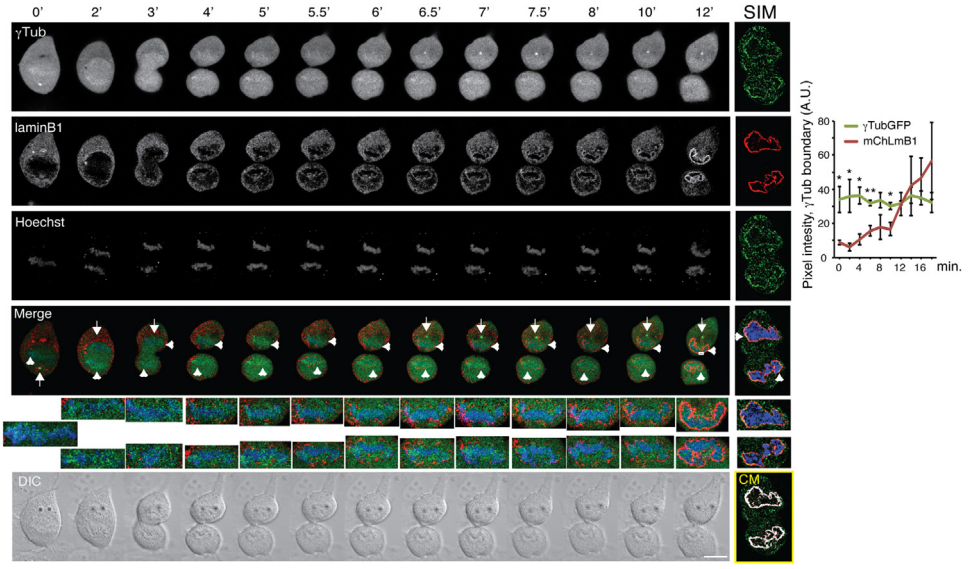

Fig. 14. Lamin B1 assembles at the γ-tubulin boundary. The DIC/fluorescence images show time-lapse series from a stable *γTUBULIN*sh-U2OS cell co-expressing GFP-γ-tubulin$_{resist}$ (γTub; green) that was transiently expressing mCherry-lamin B1 (lamB1; red). The image series show chosen frames of the lamina (laminB1) formation at the γ-string boundary (cytosolic and chromatin-associated γ-strings) formed by GFP-γ-tubulin$_{resist}$ during nuclear assembly in a mitotic cell. The mitotic chromosomes/daughter nuclei are magnified below the merged images. Arrowheads and arrows show the γ-string-boundary around the mitotic chromosomes and the mitotic spindle, respectively. The graph shows the time-dependent changes in fluorescence intensity across the white box at the γ-string-boundary of γtubGFP (green) and mCherry-lamin B1 (mChlmB1; red) expressed in arbitrary units (AU; mean ± s.d.; $n = 3$). Right, structured illumination microscope (SIM) images show immunofluorescence staining of endogenous γ-tubulin and lamin B with an anti-γ-tubulin (green; T6557) and anti-lamin B1 (red) antibody of newly formed U2OS daughter cells. Nuclei were detected with DAPI (blue). The yellow box shows colocalization pixel-map (CM) of the red and green channels. White areas in CM denote colocalized pixels between channels. Scale bars, 10 μm. See also movie S1.

intertwined with the γ-tubulin-boundary of γ-strings (Fig. 14, 4–12 min). Structured illumination microscopy confirmed the location of the γ-tubulin-boundary in the newly assembled daughter nuclei (Fig. 14), which resembled the γ-tubulin nuclear boundary formed in stage 4 in a newly assembled *X. laevis* nucleus (Fig. 4B). Similar mCherry-lamin B1 localization was observed in U2OS cells (Fig. 15A) and in *γTUBULIN*sh-U2OS cells, despite the lower expression of endogenous γ-tubulin and mCherry-lamin B1 in the latter cell line (Fig. 15B). These data further support that in living cells γ-strings may function as a scaffold meshwork that assists the formation of the lamina around mitotic chromosomes.

As the amount of GFP-γ-tubulin associated with mitotic chromosomes was higher than anticipated in *γTUBULIN*sh-U2OS-GFP-γ-tubulin$_{resist}$ cells (Fig. 14), we tested the effect of the position of the GFP-tag and the stable expression of *γTUBULIN* shRNA on the cellular location of GFP-γ-tubulin in γtubGFP-U2OS (U2OS cells that stably expressed human GFP-γ-tubulin; Fig. 16A) and in

http://dx.doi.org/10.1016/j.heliyon.2016.e00166

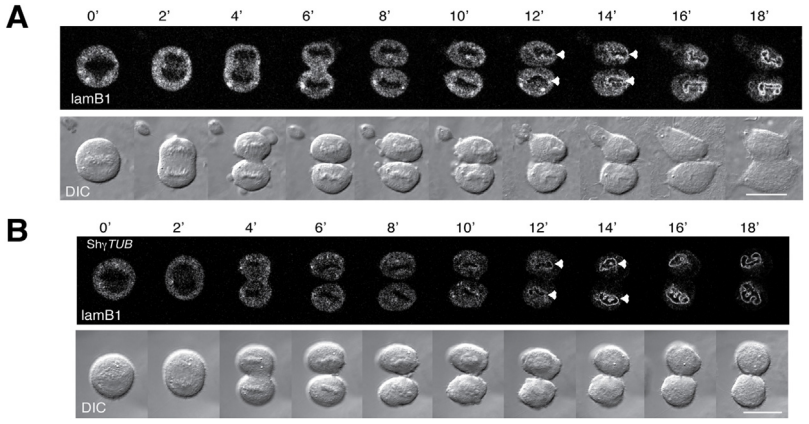

Fig. 15. Formation of the lamina in U2OS and *γTUBULIN*sh-U2OS cells. (A, B) The DIC/fluorescence images show time-lapse series from U2OS (A) and *γTUBULIN*sh-U2OS cells (B; sh*γTUB*) that were transiently expressing mCherry-lamin B1 (lamB1). The image series show chosen frames of the location of lamin B1 during nuclear assembly in a mitotic cell. Images were collected every 30 sec. Scale bars, 10 μm. Arrowheads show the formed lamina around daughter chromatids. These time-lapse movies are available at movie S2 and movie S3.

*γTUBULIN*sh-U2OS-NGFP-γ-tubulin$_{resist}$ cells (*γTUBULIN*sh-U2OS cells that stably expressed human GFP-N terminal-tagged sh-resistant γ-tubulin; Fig. 16B) and monitored the amount of chromatin-associated GFP-γ-tubulin pool by time-lapse microscopy. We noticed that the association of GFP-γ-tubulin with chromatin was independent of the position of the GFP-tag. Also, the lower the endogenous protein levels of γ-tubulin, the higher levels of chromatin-associated GFP-γ-tubulin

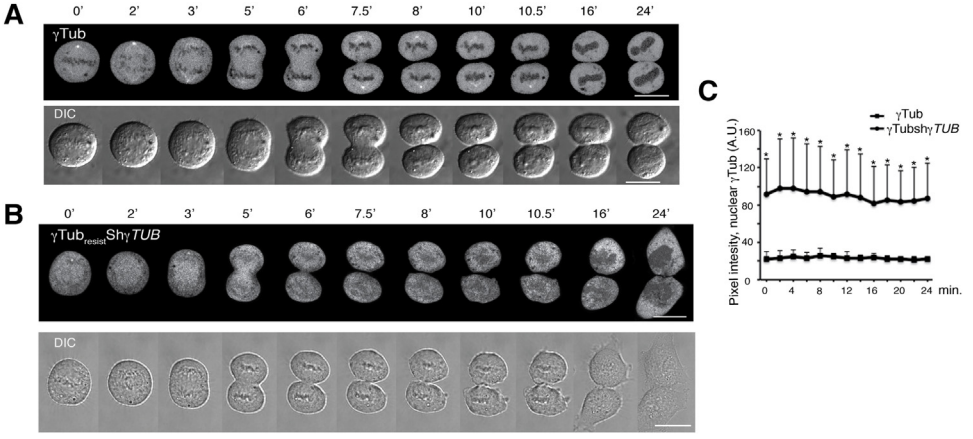

Fig. 16. The endogenous protein levels of γ-tubulin affect the association of GFP-γ-tubulin to chromatin. (A, B) The DIC/fluorescence images show time-lapse series from U2OS cells that stably expressed either C-terminal tagged GFP-γ-tubulin (γTub; A) or both *γTUBULIN* shRNA and N-terminal tagged GFP-γ-tubulin$_{resist}$ (γTub$_{resist}$Sh*γTUB*; B). The image series show chosen frames of the variation over time in the amount of chromatin-associated GFP-γ-tubulin. Images were collected every 30 sec. Scale bars, 10 μm. (C) The graph shows the time dependent changes in fluorescence intensity across the chromatin of GFP-γ-tubulin expressed in arbitrary units (AU; mean ± s.d.; $n = 3$).

http://dx.doi.org/10.1016/j.heliyon.2016.e00166

were found (Fig. 14 and Fig. 16C). These findings suggested that endogenous γ-tubulin interfered with GFP-γ-tubulin binding to chromatin and that the amount of chromatin-associated γ-tubulin might be higher than expected.

2.9. Endogenous γ-tubulin is associated to mitotic chromosomes

One plausible reason for the underestimation of the amount of chromatin-associated γ-tubulin is that available antibodies may not fully recognize this pool,

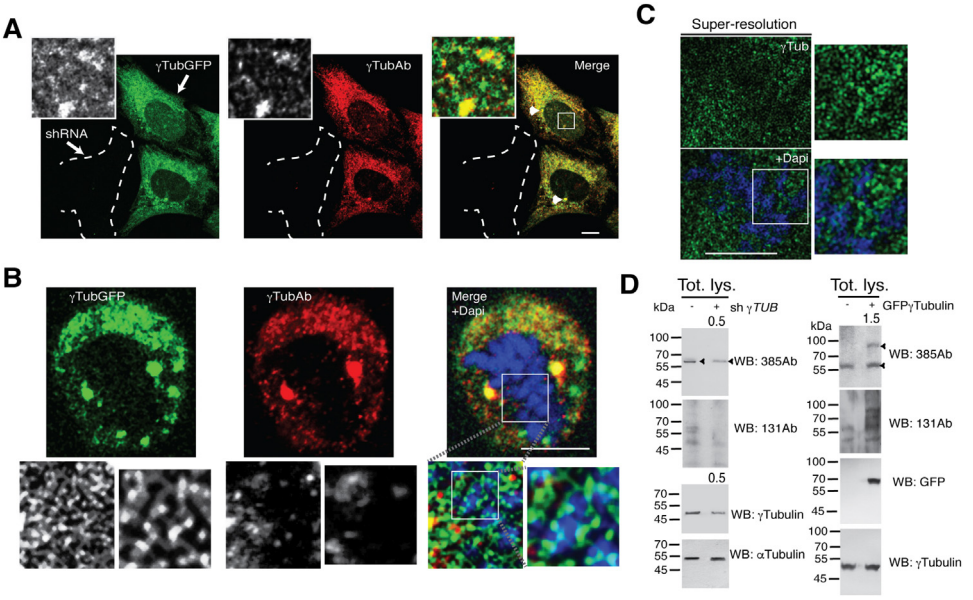

Fig. 17. Anti-γ-tubulin antibodies partially recognize chromatin-associated γ-strings. (A, B) The fluorescence images show representative images of immunostained GFP-γ-tubulin (green; γTubGFP) with an anti-γ-tubulin antibody (red; γTubAb; T3320) in interphase (A) and mitotic (B) U2OS cells stably expressing both *γTUBULIN* shRNA (shRNA) and GFP-γ-tubulin$_{resist}$ (γTubGFP). Four different antibodies were tested (ab27074, T5192, T3320 and T6557) and the one that best recognized chromatin-associated γ-tubulin (T3320) is shown. (A) The specificity of the polyclonal anti-γ-tubulin antibody (T3320) used was tested in U2OS cells stably expressing both *γTUBULIN* shRNA and GFP-γ-tubulin$_{resist}$ (*γTUBULIN*sh-U2OS-GFP-γ-tubulin$_{resist}$ cells). The dashed line follows one of three *γTUBULIN*sh-U2OS-GFP-γ-tubulin$_{resist}$ cells with low expression of both endogenous γ-tubulin and GFP-γ-tubulin$_{resist}$. Arrows and arrowheads indicate a cell with high and low expression of γ-tubulin and the location of centrosomes, respectively. (C) Structured illumination images of a fixed U2OS immunostained with an anti-γ-tubulin (T6557). (A-C) White borders show the magnified areas displayed in the insets. Scale bars, 10 μm. (B, C) Nuclei were detected with DAPI (blue). (D) Total lysate from U2OS and U2OS cells stably expressing *γTUBULIN* shRNA (sh*γTUB*) or NGFP-γ-tubulin were first analyzed by WB with a polyclonal anti-γ-tubulin antibody (385Ab) and reprobed with a polyclonal anti-γ-tubulin antibody (131Ab), a mixture of two anti-γ-tubulin (T5192 and T3320) or of two anti-GFP antibodies (sc-53882 and sc-8334) and an anti-α-tubulin antibody. Arrowheads indicate the 60-kDa and the 90-kDa bands recognized by 385Ab ($n = 3$). Numbers on WBs indicate the level of depletion or enrichment of the amount or proteins recognized by the indicated antibody relative to control. To adjust for differences in protein loading, the protein concentration of the indicated proteins was determined by its ratio with endogenous γ-tubulin for each sample. The protein ratio in control extracts was set to 1.

http://dx.doi.org/10.1016/j.heliyon.2016.e00166

as previously reported (Eklund et al., 2014). Indeed, interphase (Fig. 17A) and mitotic (Fig. 17B) γ-tubulin immunostained *γTUBULIN*sh-U2OS-GFP-γ-tubulin-$_{resist}$ cells showed that the antibody recognized only part of the chromatin-associated pool (Fig. 17A, B). Nonetheless, structured illumination microscopy detected the chromatin-associated γ-tubulin pool in mitotic cells (Fig. 17C), confirming the association of γ-tubulin with mitotic chromosomes.

To obtain an antibody that better recognized chromatin-associated γ-tubulin, we generated a polyclonal rabbit antibody (385Ab) to the γ-tubulin region containing Ser^{385} (residues 372 to 389), as phosphorylation of this residue induces a change in the conformation of γ-tubulin that causes a size shift from 49 kDa to 60 kDa in SDS gels originating a protein band that is recognized by neither commercially available anti-γ-tubulin nor anti-GFP antibodies (Fig. 17D) (Eklund et al., 2014). The 385Ab recognized a 60-kDa band, which signal was reduced upon reduced protein levels of γ-tubulin (Fig. 17D), demonstrating that the identified protein band was γ-tubulin. Furthermore, the 385Ab recognized an additional 90-kDa band in U2OS cells stably expressing Nγ-tubGFP that was neither recognized by anti-γ-tubulin or anti-GFP antibodies, but were recognized by antibodies generated to the γ-tubulin region containing Ser^{131} (Eklund et al., 2014). Altogether, the data proves that the GFP-tagged γ-tubulin and γ-tubulin undergo the same conformational change (Fig. 17D).

Immunofluorescence analysis showed that in comparison to other anti-γ-tubulin antibodies (Fig. 17A), 385Ab only stained partially the γ-tubulin pools associated with centrosomes and microtubules (Fig. 18A, B), but recognized instead a γ-tubulin pool that was evenly distributed throughout interphase and mitotic cells (Fig. 18A, B). Moreover, the immunofluorescence staining recognized with 385Ab was decreased in U2OS cells expressing *γTUBULIN* shRNA (Fig. 18B). Finally, immunoelectron microscopy of U2OS cells using 385Ab showed that the antibody fully recognized γ-tubulin bridges (Fig. 18C) and cytosolic and nuclear γ-strings (Fig. 18D). The data presented here confirm that during cell division, there is a γ-tubulin boundary formed of γ-strings around chromatin (Fig. 18E).

2.10. Formation of chromatin-containing nuclei depends on the DNA-binding domain of γ-tubulin

The observation that the C-terminal DNA-binding domain of γ-tubulin (Hoog et al., 2011) is the necessary domain for the formation of a nuclear membrane and a lamina in *X. laevis* egg extracts prompted us to investigate the role of γ-tubulin's N- (residues 1–333) and C-terminal (residues 334–452) regions in nuclear formation in U2OS cells.

We first investigated the γ-tubulin domain necessary in the γ-tubulin–lamin complex by analyzing GFP immunoprecipitates from *γTUBULIN*sh-U2OS cells

http://dx.doi.org/10.1016/j.heliyon.2016.e00166

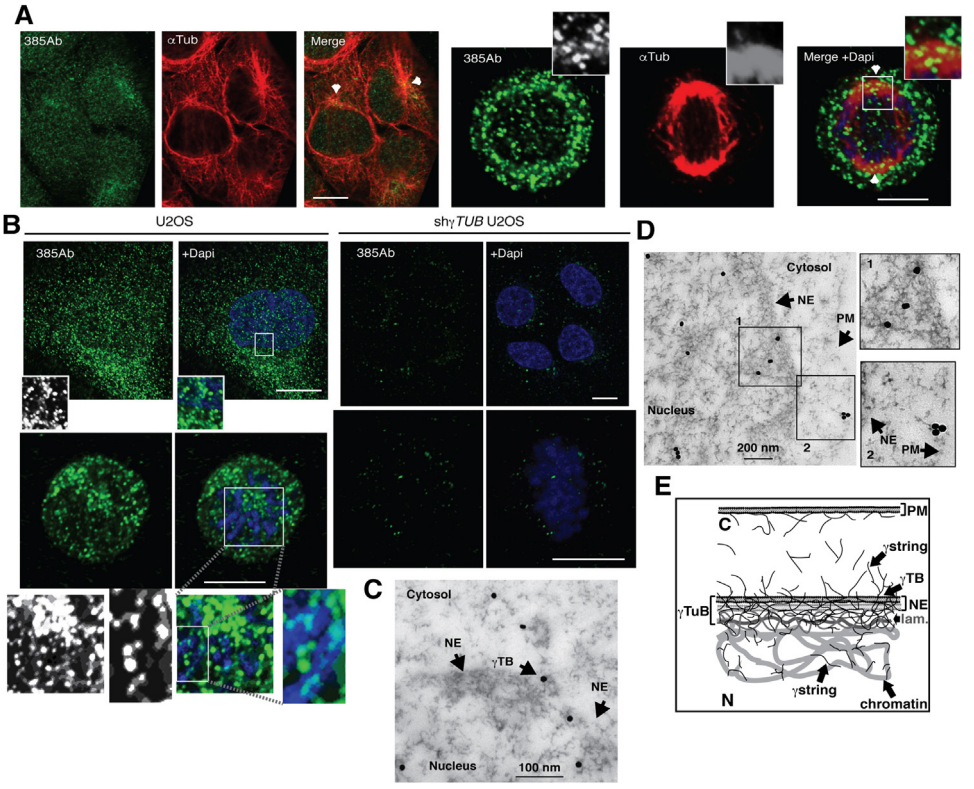

Fig. 18. Anti-γ-tubulin antibodies against Ser^{385}-γ-tubulin recognize chromatin-associated γ-strings. (A, B) The fluorescence images show representative images of immunostained U2OS and stable *γTUBULIN*sh-U2OS cells with 385Ab (green) in interphase and mitosis. Nuclei were detected with DAPI (blue). Scale bars, 10 μm. (A) Microtubules and centrosomes were stained with an anti-α-tubulin antibody (red). Arrowheads indicate the location of centrosomes. (C, D) Endogenous γ-tubulin detection in immunoelectron microscopy using 385Ab. Images show the plasma membrane [PM], cytosol, nuclear envelope [NE] and γ-tubulin bridges [γTB] of an interphase U2OS cell. (A-D) White and black boxes show the magnified areas displayed in the insets. (E) The γ-string meshwork is composed of treads (γ-string), which are attached to the plasma membrane [PM], found in the cytosolic [C] compartment and enter into the nuclear compartment [N] through the nuclear envelope [NE]. In the nuclear compartment, γ-strings are intertwined with the lamina [lam.] meshwork and with chromatin. γ-Tubulin bridges [γTB] connect the cytosolic and the nuclear γ-tubulin pools creating a nuclear boundary of γ-tubulin [γTuB].

stably expressing one of the following constructs: GFP-γ-$tubulin_{resist}$, N-terminal (NγtubGFP$^{1-333}$; *γTUBULIN*sh-U2OS-GFP-Nγ-tubGFP$^{1-333}$) and C-terminal (CγtubGF$P_{resist}{}^{334-452}$; *γTUBULIN*sh-U2OS-GFP-Cγ-tubGFP$^{334-452}$) region of γ-tubulin (Fig. 19A). Both CγtubGFP$^{334-452}$ and NγtubGFP$^{1-333}$ were associated with lamins (Fig. 19A), which imply that both regions contain necessary sequences for the formation of the γ-tubulin–lamin complex. It also suggested that the N-terminal region of γ-tubulin might be sufficient for triggering lamina formation.

To understand the impact of the interactions of the N-terminal region of γ-tubulin with lamin B1 on lamina formation in U2OS cells, we monitored mitotic

http://dx.doi.org/10.1016/j.heliyon.2016.e00166

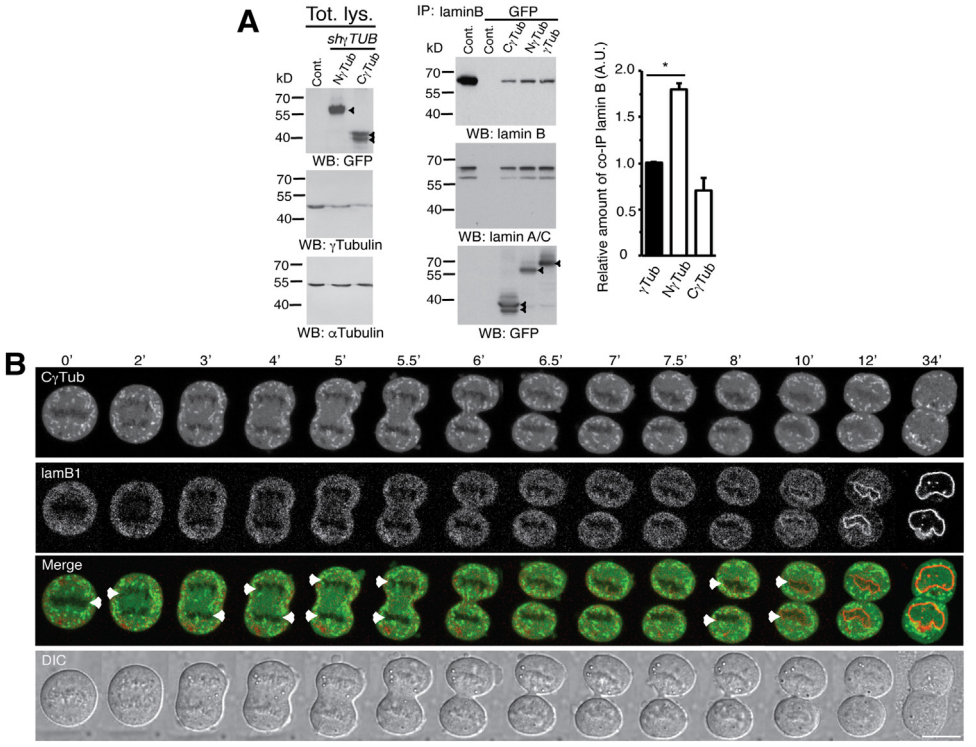

Fig. 19. The C-terminal region of γ-tubulin assures the formation of chromatin-containing nuclei. (A) Total lysate from U2OS cells expressing C-γtubGFP$^{334–452}$ (CγTub), N-γtubGFP$^{1–333}$ (Nterm), GFP-γ-tubulin (γTub) or empty vector (Cont.) were separately immunoprecipitated with anti-GFP or anti-lamin B. The expression levels of the various recombinant proteins were first analyzed by WB with an anti-GFP and reprobed with a mixture of two anti-γ-tubulin (T3320 and T6557) antibodies. The cellulose membranes containing immunoprecipitated GFP-tagged proteins were first analyzed by WB with an anti-lamin B antibody and reprobed with an anti-lamin A/C and −GFP. Arrowheads indicate the immunoprecipitated GFP-fused proteins (n = 3). Graph shows the protein concentration of lamin B found in C-γtubGFP$^{334–452}$ and N-γtubGFP$^{1–333}$ immunoprecipitates relative to the lamin B concentration found in GFP-γ-tubulin immunoprecipitates expressed in arbitrary units (AU; mean ± s.d; n = 3, * $p < 0.05$). To adjust for differences in protein loading, the protein concentration of lamin B was determined by its ratio with the immunoprecipitated GFP-tagged protein for each sample. The protein ratio in control extracts was set to 1. (B) DIC/fluorescence images of time-lapse from a U2OS cell that is stably expressing both *γTUBULIN* shRNA and sh-resistant Cγ-tubGFP$^{334–452}$ (CγTub, green), and transiently expressing mCherry-lamin B1 (lamB1; red) with Hoechst 33258 stained chromatin (blue), as indicated. The image series show chosen frames of the location of Cγ-tubGFP$^{334–452}$ and lamin B1 during nuclear assembly in a mitotic cell. Images were collected every 30 sec. Scale bars, 10 μm. See also movie S4.

*γTUBULIN*sh-U2OS-GFP-Cγ-tubGFP$^{334−452}$ and *γTUBULIN*sh-U2OS-GFP-Nγ-tubGFP$^{1−333}$ (Eklund et al., 2014; Hoog et al., 2011) cells that transiently co-expressed mCherry-lamin B1 by time-lapse microscopy. Mitotic U2OS cells expressing Cγ-tubGFP$^{334−452}$ divided similarly to *γTUBULIN*sh-U2OS-GFP-γ-tubulin$_{resist}$ cells (Fig. 14 and Fig. 19B; movie S4; n = 16). By contrast, in 39% (13 cells) of the studied mitotic *γTUBULIN*sh-U2OS-GFP-Nγ-tubGFP$^{1−333}$ cells (n = 33), daughter cells formed an additional lamina in the absence of

http://dx.doi.org/10.1016/j.heliyon.2016.e00166

chromatin (movie S5; Fig. 20A, 6–59 min). Moreover, we found chromatin empty nuclear like structures in 15% of interphase cells stably expressing N-γtubGFP (4 ± 1%, $n = 3$; Fig. 20B). Together, our results demonstrate that both the N- and C-terminal regions of γ-tubulin assist in the formation of the lamina, but only the DNA-binding C terminus has the ability to assure the formation of a lamina around chromatin.

3. Discussion

Here we show that γ-tubulin is an important coordinator of cytosolic and nuclear events that leads to the formation of the nuclear membrane and the lamina in the two daughter cells. γ-Tubulin forms cytosolic and chromatin-associated γ-strings, which we suggest both give support to the emerging nuclear membrane and assure the formation of a nuclear envelope around daughter chromatids. Immunodepletion of γ-tubulin impaired nuclear formation in *X. laevis* egg extracts and addition of

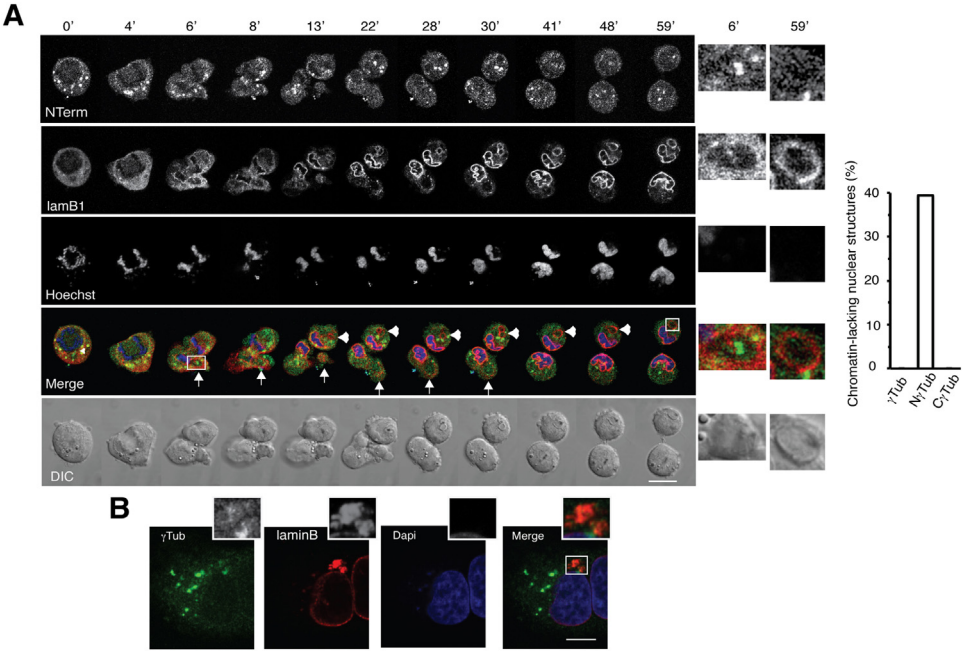

Fig. 20. The N-terminal region of γ-tubulin leads to the formation of chromatin-empty nuclei. (A) DIC/fluorescence images of time-lapse from a U2OS cell that is stably expressing both *γTUBULIN* shRNA and sh-resistant N-γtubGFP$^{1–333}$ (NTerm, green), and transiently expressing mCherry-lamin B1 (lamB1; red) with Hoechst 33258 stained chromatin (blue), as indicated. The image series show the location of N-γtubGFP$^{1–333}$ and lamin B1 in a mitotic cell that during nuclear assembly transiently formed two nuclear-like structures, which lack chromatin (arrowhead and arrow). Chromatin-lacking nuclear-like structures (white borders) are shown on the right images. Graph shows the percentage of filmed cells that formed chromatin lacking nuclear like structures. Images were collected every 30 sec. See also movie S5. (B) Fixed U2OS cells that are stably expressing *γTUBULIN* shRNA and N-γtubGFP$^{1–333}$ were immunofluorescence stained with an anti-lamin B antibody (laminB; red) and nuclei were detected with DAPI (blue). (A, B) Scale bars, 10 μm.

http://dx.doi.org/10.1016/j.heliyon.2016.e00166

γ-tubulin or its C-terminal region reversed this effect. The effect of γ-tubulin on nuclear assembly is based on γ-tubulin's ability to directly bind to the sperm chromatin and to facilitate lamina and nuclear membrane formation. In mammalian cell lines, γ-tubulin forms γ-strings and the nuclear envelope emerged at the γ-tubulin boundary composed of cytosolic and chromatin associated γ-strings. *In vitro*, γ-tubulin forms strings that support formation of lamin B3 protofilaments and the lamina is disassembled in cells with decreased protein levels of γ-tubulin. Finally, although both γ-tubulin's N and C terminus induce the formation of a lamina, only the DNA-binding domain of γ-tubulin can build up a functional nucleus (Hoog et al., 2011). Thus, we propose that the interaction of lamins with the N-terminal region of γ-tubulin probably connects lamin–γ-tubulin complexes with the cytosolic γ-tubulin pool, whereas the C-terminal region links lamin–γ-tubulin with chromatin.

To our knowledge we are the first group showing the formation of a lamina in the absence of chromatin. Studies performed with *X. laevis* egg extracts demonstrate that lamina formation occurs only around chromatin (Lopez-Soler et al., 2001). A possible explanation for the discrepancy is that in the *X. laevis* egg extracts, a cytosolic γ-string boundary around the emerging nucleus is first formed once the nucleus is assembled. Thus, the lack of a preformed cytosolic γ-string boundary will prevent formation of chromatin-empty nuclear like structures. By contrast, in cells, the cytosolic γ-string boundary around chromosomes and chromatin-associated γ-strings are never disassembled during cell division and thereby the boundary between cytosolic and chromatin-associated γ-strings assures the formation of a lamina around mitotic chromosomes.

Although the functions of γ-tubulin have been extensively studied over the past decades, there are not previous reports on γ-strings. There are two possible reasons for this. First, most of studies performed on γ-tubulin focus on examining the function of γ-tubulin as a centrosome and microtubule organizer and most of the antibodies commercially available are selected for the recognition of those γ-tubulin pools. Second, γ-tubulin is an abundant cellular protein that is found in both the cytosol and the nuclear compartment. This type of meshwork is difficult to stain and the staining is difficult to interpret as the antibody stains both the cytoplasm and the nucleus. An example of a meshwork easy to stain is microtubules. α- and β-tubulins form distinct cytosolic fibers (25 nm in diameter), which are easily detected with antibodies. The low concentration of soluble α- and β-tubulins surrounding the arrays enhances their staining. In contrast, γ-strings differ from previous described meshwork, as these are fine structures that are distributed in both the cytosolic and the nuclear compartment. The lack of areas with low concentration of γ-strings makes it difficult to detect their structure.

http://dx.doi.org/10.1016/j.heliyon.2016.e00166

The mechanisms that regulate γ-string formation require further analysis. Nonetheless, *in vitro* γ-tubulin forms strings in the absence of GTP and in cells, in the absence of the GTPase domain of γ-tubulin, the C-terminal region forms tubule-like structures in a Ser 385-γ-tubulin dependent manner (Eklund et al., 2014). Thus, one can speculate that γ-tubulin polymerization depends on C-terminal-to-C-terminal binding and the N-terminal region regulates its dynamics.

Our results suggest that the interplay between the cytosolic and the chromatin-bound γ-strings across the nuclear envelope plays an important role during cell cycle. We propose the following model. During interphase, γ-tubulin bridges connect the cytosolic and the nuclear γ-tubulin pools. At the onset of mitosis, the lamina meshwork is disrupted (Collas, 1999; Peter et al., 1990), but the γ-tubulin boundary around the mitotic chromosomes is maintained. During mitosis, chromatin-associated γ-strings link the sister chromatids to the cytosolic γ-string pool. Finally, at anaphase/telophase, the γ-tubulin boundary composed of cytosolic and chromatin associated γ-strings forms a supporting scaffold that assist the formation of the nuclear envelope.

Recently, an association of γ-tubulin with the nucleoporin MEL-28/ELYS and the nuclear envelope re-assembling GTPase, Ran, has been described (Yokoyama et al., 2014). In addition, γ-tubulin associated proteins such as αβ-tubulin and the γ-tubulin complex protein 3-interacting proteins shape the nuclear envelope (Batzenschlager et al., 2013; Xue et al., 2013). These data together with the data presented here suggest that the γ-tubulin meshwork may be a structuring scaffold that favors the nucleation of various protein complexes necessary for nuclear formation.

Overall, our results suggest a novel mechanism for how γ-tubulin coordinates cytosolic and nuclear events during cell cycle.

4. Materials and methods

4.1. cDNA, proteins and antibodies

Y. Zheng (Ma et al., 2009; Martin et al., 1998) and M. Klymkowsky (Dent et al., 1989) provided lamin B3 pET-28a His_6-tagged and anti-lamin B3, anti-Xgrip109 and anti-lamin II/III antibodies (1:25). *TUBULIN* shRNA, sh-resistant *γ*-TUBULIN-1 gene, Nγ-tubGFP (γ-$tubulin_{1–333}$), Cγ-tubGFP (γ-$tubulin_{334–452}$), His_6–γ-tubulin, His_6–γ-$Tub_{335–451}$, His_6–E2F1 (Δ194-426) and GFP-$SADB_L$ were prepared as reported (Alvarado-Kristensson et al., 2009; Eklund et al., 2014; Hoog et al., 2011). Human N-terminal GFP-tagged γ-tubulin and N-terminal γ-tubulin fragment (His_6–γ-$Tub_{1–334}$) were obtained by PCR from γ-tubulin/pEGFP-N1 (Alvarado-Kristensson et al., 2009) and subcloned in-frame into pEGFP-C1 (Clontech) or into pET21d (Novagen), respectively, using the

http://dx.doi.org/10.1016/j.heliyon.2016.e00166

following primers: 5′GCGAAGCTTCGATGCCGAGGGAAATCATC3′ and 5′GCGGAATTCTCACTGCTCCTGGGTGCCCCAGGAGAT3′ (γ-tubulin); 5′GCGGAATTCGTATGCCGAGGGAAATCATCACC3′ and 5′CGCAAGCTTGACCTGGGTGGGGT3′ (His_6–γ-$Tub_{1–334}$). Human RBM3 was amplified from human cDNA and PCR RBM3 was subcloned in-frame into pEGFP-N1 (Clontech) using the following primers: 5′GCGGCTAGCGACCATGTCCTCTGAAGAAGGAAAG3′ and 5′GCGAAGCTTTTTCATGTTGTCATAATTGTCTCTGT3′. The constructs were verified by sequence analysis.

The following reagents were used: human N-terminal mCherry tagged Lamin B1/pReceiver-M55 (GeneCopoeia, Rockville, USA), anti-lamin B2, anti-laminA/C, anti-centrin 2 (1:250; sc-27793), anti-histone 2B (1:500), anti-histone 3 (1:200), anti-GFP (sc-53882 and sc-8334; 1:500), mouse anti-γ-tubulin (1:400; sc-51715) and rabbit anti-α-tubulin (1:400, all from Santa Cruz Biotechnology, Dallas, Texas, USA), mouse and rabbit anti-γ-tubulin (1:250–400, Sigma-Aldrich, Munich, Germany; T5192, T3320 and T6557), anti-γ-tubulin (1:400; ab27074) and anti-His_6 (1:1000, Abcam, Cambridge, UK), anti-α-tubulin (1:400, Millipore, Temecula, California, USA), anti-nuclear pore complex (1:250, Covance, New Yersey, USA), anti-GFP (1:500) and anti-lamin B (1:500, both from Santa Cruz Biotechnology, Dallas, USA). Other reagents used included protein G PLUS-sepharose (GE Healthcare, Cleveland, USA) and SDS-PAGE reagents (Bio-Rad, California, USA). All other reagents were obtained from Sigma-Aldrich.

A rabbit anti-γ-tubulin antibody was generated using the phosphopeptide RVSGLMMANHTSI<u>S</u>SLFE (phosphorylated S underlined; Pacific Immunology, California, USA). The anti-total-γ-tubulin antibody (1:400) was purified using a matrix coupled covalently to the non-phosphorylated peptide, as described (Alvarado-Kristensson et al., 2009).

4.2. Manipulation of Xenopus laevis eggs and sperm

The Ethics Committee of Lund University approved the study (reference number: M 151–11). Interphase (CSF-arrested) egg extracts were prepared in CSF-XB buffer (10 mM HEPES-KOH pH 7.7, 50 mM sucrose, 0.1 M KCl, 1 mM $CaCl_2$, 2 mM $MgCl_2$) supplemented with 0.1 mg/ml cytochalasin B as described (Murray, 1991) with the following modifications to improve the quality of the egg extracts: ovulation was induced injecting 600 units of human chorionic gonadotrophin (Sigma); paraffin oil was used; and, after crushing, the supernatant was centrifuged at 10,000 g for 12 min to remove remaining debris. Finally, interphase egg extracts were obtained by supplementation with the calcium ionophore A23187 (sigma) (Losada et al., 1998).

http://dx.doi.org/10.1016/j.heliyon.2016.e00166

Demembranated sperm were prepared as previously described (Murray, 1991) using benzocaine 0.05% (W/V) as an anesthetic with the following modifications. To remove possible membrane fragments; cytosolic components and contaminating microtubules, sperms were pelleted by centrifugation (18,000 g, 2 min) onto a 200 µl cushion containing SuNaSp, 1.3 M and glycerol (Felix et al., 1994). Occasionally, previous centrifugation onto the glycerol cushion, sperm were prepared in the presence of 5 µg/ml colcemid and 2.5 µg/ml cytochalasin B (Murray, 1991). Reactions with interphase egg extracts and sperm were incubated at 22 °C. Immunodepletion were performed twice as described (Ma et al., 2009) using each time 5 µl of anti-γ-tubulin T3320, anti-lamin B3 or no antibody (control depletion). Demembranated sperm was depleted from proteins (Ksperm) by treatment with 0.25 mg/ml proteinase K for 17 min at 37 °C. Reactions were stopped by placing samples on ice and adding 30 mg/ml glycine, 0.4 mM phenylmethanesulfonyl fluoride and 0.38% BSA.

For add-back experiments, human His_6-tagged fusion proteins (His_6–γ-tubulin, His_6–γ-$Tub^{1–334}$, His_6–γ-$Tub^{335–451}$ and His_6–E2F1 [Δ194-426]) and *Xenopus* His_6-tagged lamin B3 (Ma et al., 2009) were expressed as described (Hoog et al., 2011; Tsai et al., 2006). 100 ng of recombinant proteins were added to the immunodepleted egg extracts or pre-incubated with Ksperm for 10 min prior to addition of egg extract. 500 sperm/µl extract was used in assembly reactions. To analyze the functionality of the various recombinant His_6–γ-tubulin proteins, formed nuclei were spun down (2,800 g) through a cushion of 30% sucrose (w/v) in BAD (Mendez and Stillman, 2000) and pellets were lysed and analyzed as previously described (Alvarado-Kristensson et al., 2002).

To test the specificity of the antibodies used, recombinant His_6–γ–tubulin affinity pre-bound to Ni2+ affinity resin (Qiagen) was incubated in the presence of the antibodies T3320 or ab27074 for 2 h before immunostaining demembranated sperm.

4.3. Expression and purification of recombinant proteins

The human C-terminal His_6-tagged fusion proteins (His_6-γ-tubulin, His_6-γ-$Tub_{1–334}$ and His_6-γ-$Tub_{335–451}$) were expressed in *Escherichia coli* BL21 (DE3) (Stratagene) as described previously (Hoog et al., 2011). The *Xenopus* N-terminal His_6-tagged lamin B3 fusion proteins were produced in *E. coli* BL21 (DE3) as described elsewhere (Tsai et al., 2006). In brief, exponentially growing bacteria bearing the plasmid were maintained at room temperature overnight (His_6-tagged lamin B3) or at 37 °C for 1 h (His_6-γ-tubulin, His_6-γ-$Tub_{1–334}$ and His_6-γ-$Tub_{335–451}$). Recombinant proteins were purified under native conditions using Ni^{2+} affinity resin (Qiagen), in binding buffer (His_6-tagged lamin B3: 50 mM Tris-HCl pH 8.0, 25% sucrose, 1% TritonX-100, 1 mM PMSF, and 5 mM imidazole;

http://dx.doi.org/10.1016/j.heliyon.2016.e00166

His_6-γ-tubulin, His_6-γ-$Tub_{1–334}$ and His_6-γ-$Tub_{335–451}$: 20 mM Tris-HCl pH 7.9, 500 mM NaCl, 1 mM $MgCl_2$, 0.25 μM GTP, 5 mM beta-mercaptoethanol (βME), 1 mM PMSF and 5 mM imidazole). Then the proteins were washed in 50 mM Tris-HCl pH 8.0 and 60 mM imidazole (His_6-tagged lamin B3) or in 20 mM Tris-HCl pH 7.9, 1 mM $MgCl_2$, 0.25 μM GTP, 5 mM βME and 60 mM imidazole (His_6-γ-tubulin, His_6-γ-$Tub_{1–334}$ and His_6-γ-$Tub_{335–451}$) and eluted in 50 mM Tris-HCl pH 8.0 and 1 M imidazole (His_6-tagged lamin B3) or in 20 mM Tris-HCl pH 7.9, 500 mM NaCl, 1 mM $MgCl_2$, 0.25 μM GTP, 5 mM βME and 1 M imidazole (His_6-γ-tubulin, His_6-γ-$Tub_{1–334}$ and His_6-γ-$Tub_{335–451}$). The purified proteins were exchanged into XB (His_6-tagged lamin B3: 10 mM HEPES, pH 7.7, 50 mM sucrose, 100 mM KCl, 0.1 mM $CaCl_2$, and 5 mM EGTA) or TAB (His_6-γ-tubulin, His_6-γ-$Tub_{1–334}$ and His_6-γ-$Tub_{335–451}$: 40 mM K-HEPES, 150 mM NaCl, 1 mM $MgCl_2$, 1 mM EGTA and 1 mM DTT, at pH 7.2) buffer using a dialysis membrane (SpectrumLabs) and concentrated in an Amicon Ultra Centrifugal Filter (Millipore).

4.4. *In vitro* γ-string and lamin B3 polymerization assays

γ-Strings, lamin B3 fibers or both were polymerized by incubating 20 μM His_6-γ-tubulin (Alvarado-Kristensson et al., 2009; Eklund et al., 2014; Hoog et al., 2011; Ma et al., 2009), 600 nM His_6-lamin B3 (Ma et al., 2009) or both proteins for 1 h at 22 °C with the following buffers: γ-tubulin assembly buffer (TAB), lamin B3 assembly buffer (LAB: TAB, supplemented with 10 mM sucrose, 20 mM KCl and 20 μM $CaCl_2$). The ability of His_6-γ-tubulin to assist the formation of His_6-lamin B3 fibers was tested in LAB buffer. The assembled meshwork was fixed using 1% of glutaraldehyde for 5 min. In some experiments TAB was supplemented with 1 mM GTP.

4.5. Cell culture, transfection, immunoprecipitation and fractionation

NIH3T3 mouse fibroblast and U2OS human osteosarcoma cells were cultured transfected and fractionated as reported (Alvarado-Kristensson et al., 2009; Eklund et al., 2014; Hoog et al., 2011). Proteins in purified cellular fractions or cell lysates were immunoprecipitated as described (Eklund et al., 2014) with the following modifications. Before immunoprecipitation, chromatin-associated complexes were released from chromatin by resuspending the chromatin pellets in chromatin degrading buffer (2 units/μl benzonase [Sigma], 20 ng/μl Dnase I [Sigma], 50 mM Tris pH 7.5, 150 mM NaCl, 2 mM $MgCl_2$) for 15 min, 22 °C. Western blotting was performed as reported (Alvarado-Kristensson et al., 2002).

http://dx.doi.org/10.1016/j.heliyon.2016.e00166

Stably transfected *γTUBULIN* shRNA U2OS cells and the various U2OS cell lines stably expressing GFP-γ-tubulin (C- or N-tagged γ-tubulin), NGFP-γ-tubulin or CGFP-γ-tubulin were obtained as described (Lindstrom et al., 2015).

To isolate nuclei, cells were pre-incubated for 20 min with culture medium containing 100 ng/ml colcemid and 5 μg/ml cytochalasin B (37 °C, 5% CO_2) to release cytoskeletal components from nuclei and cytoplasm. Nuclei of harvested cells were incubated for 5 min in BAD (Mendez and Stillman, 2000) containing 0.1% triton X–100. Nuclei were fixed for 15 min at room temperature with 4 volumes of 10% formaldehyde in BAD and then spun (2,400 g) onto coverslips through a cushion of 30% sucrose (w/v) in BAD.

4.6. Fluorescence imaging microscopy

Immunostaining of demembranated sperm were performed by first air-drying sperm and thereafter were fixed for 3 min with methanol/acetone (1:1; v/v) at −80 °C. Nuclear assembly was ended by addition of 4 volumes of 10% formaldehyde in MMR (Murray, 1991) or 2% formaldehyde supplemented with 0.25% Triton-X100 in XBE2 (Losada et al., 1998). Fixed nuclei were spun onto coverslips through a cushion of 30% sucrose (Losada et al., 1998). Subsequent immunostaining was performed as described (Alvarado-Kristensson et al., 2009; Brown et al., 1995). The integrity of the nuclei formed was visualized by exclusion of 0.1 mg/ml 155-kD tetramethylrhodamine isothiocyanate (TRITC)-labeled dextran, as described (O'Brien and Wiese, 2006).

Cells were cultured on coverslips and to confirm the presence of γ-strings under various fixation conditions, we used three different fixation procedures. First, cells were fixed and permeabilized in methanol/acetone (1:1; −80 °C, 5 min), second, cells were fixed in 4% paraformaldehyde (PFA; RT, 5 min) and permeabilized in 0.1% Triton-X100, and third, cells were fixed in 4% PFA-2% sucrose (RT, 3 min), followed by permeabilization in methanol/acetone (1:1; −80 °C, 3 min). Cells were incubated (1 h) with Alexa480- or Cy3-labelled secondary antibody (Jackson). Capturing of fluorescence and confocal images were performed using an Olympus IX73 microscope (Olympus, Tokyo, Japan) and a Zeiss Axio Observer microscope (Zeiss, Jena, Germany), respectively, as previously described (Alvarado-Kristensson et al., 2009; Hoog et al., 2011). Super-resolution images were captured with an ELYRA PS. 1 SIM/PALM super-resolution structured illumination (SR-SIM; Zeiss). A minimum of 100 nuclei was counted in each sample, and the percentage of isolated nuclei with lamin B1 staining or of formed nuclei was calculated.

Near simultaneous GFP/mCherry/pmTurquoise2/DIC imaging sequences were collected as described (Eklund et al., 2014; Lindstrom et al., 2015). Time-lapse images were captured every 2 min or 30 sec. Time intervals of the mitotic processes were determined by counting film frames. DNA was stained for 1 h with

http://dx.doi.org/10.1016/j.heliyon.2016.e00166

1 μg/ml Hoechst 33258. Quantification of fluorescence of chromatin-associated GFP-tagged γ-tubulin constructs was performed with ImageJ (Fiji) software (National Institutes of Health, USA).

4.7. Electron microscopy

For high pressure freezing, U2OS cells were seeded to 100% confluence onto carbon coated (10 nm) 6 mm sapphire discs (Leica) in 12-well dishes (Nunc). Cells were cryo-preserved with high pressure freezing (HPM100, Leica) followed by freeze substitution (Leica AFS2, Leica) for 48 h at −90 degrees in Acetone with 0.1% Uranyl Acetate and embedded in Lowicryl with polymerization at −25 degrees for 48 h. 60 nm sections were cut with Leica Ultracut UC7 (Leica, Vienna, Austria) and collected on one whole formvar coated carbon grids and 200 mesh Nickel grids. The sections were pre-incubated for 30 min with pre-incubation buffer (50 mM glysine, 0.1% sodium borhydride $NaBH_4$, 0.05 M Tris pH 7.4, 0.1% Triton), before incubation with polyclonal anti-γ-tubulin or anti-α-tubulin antibody in TBST (0,05 M Tris pH 7.4, 0.1% Triton, 1% BSA) for 2 hours at room temperature, followed by 1 h incubation with gold conjugated protein A (1:100, 10 nm gold; Agar Scientific, Essex, UK) in TBST. Final staining was performed with filtered 0.5% uranyl acetate for 10 min.

For paraformaldehyde fixation, cells grown on tissue culture treated polycarbonate membranes (Corning-Costar, NY, USA) were fixed with 4% paraformaldehyde (5 min). Samples were low temperature embedded in Lowicryl HM20 (EMS, PA, USA) in Leica AFS and sectioned into 50 nm ultrathin sections for transmission electron microscopy on a Leica EM UC7 (Leica Microsystems GmbH, Wetzlar, Germany) before transferring to gold grids (EMS, PA, USA). Sections were blocked in PBS and 0.5% BSA (30 min), incubated with polyclonal anti-γ-tubulin or anti-γ-tubulin 385 antibodies (both 1:100, 1 h) followed by goat-anti-rabbit IgG (20 or 10 nm gold; 1:20, 60 min; Agar Scientific, Essex, UK). Final staining was performed with filtered 4% uranyl acetate. For meshwork staining, carbon-coated copper grids were glow discharged. The polymerization assays (5 μl) were applied on each grid for 5 min. Grids were twice washed with water for 1 min, and then 5 μl of freshly filtered 1% uranyl acetate were applied for 30 s. Excess stain was wicked off with filter paper, and grids were allowed to dry at room temperature. Images were obtained using a Fei Tecnai Spirit transmission electron microscope (Fei, Hillsboro, Oregon, USA) and SIS Veleta (2 × 2k) CCD camera (Olympus, Tokyo, Japan).

http://dx.doi.org/10.1016/j.heliyon.2016.e00166

4.8. Statistical analysis

All data are expressed as means ± s.d., and statistical significance of the differences between two groups or several groups was analyzed by paired Student's t test: * $p < 0.05$, ** $p < 0.01$.

Declarations

Author contribution statement

Catalina Ana Rosselló, Lisa Lindström, Johan Glindre, Greta Eklund: Performed the experiments; Analyzed and interpreted the data.

Maria Alvarado-Kristensson: Conceived and designed the experiments; Performed the experiments; Analyzed and interpreted the data; Wrote the paper.

Funding statement

This work was supported by the Swedish Cancer Society; the Swedish childhood cancer foundation; the Royal Physiographic Society in Lund; Gunnar Nilsson; Crafoordska and the Skane University Hospital in Malmö Cancer Research Fund.

Competing interest statement

The authors declare no conflict of interest.

Additional information

Supplementary content related to this article has been published online at 10.1016/j.heliyon.2016.e00166.

ACKNOWLEDGEMENTS

We thank Y. Zheng and M. Klymkowsky for reagents, Lund University Bioimaging Center and Core Facility for Integrated Microscopy, Faculty of Health and Medical Sciences, University of Copenhagen for support with electron microscope and Centre for cellular imaging at the Sahlgrenska Academy, University of Gothenburg for support with 3D super-resolution structured illumination microscope and Elevate Scientific for editorial assistance.

References

Alvarado-Kristensson, M., Porn-Ares, M.I., Grethe, S., Smith, D., Zheng, L., Andersson, T., 2002. p38 Mitogen-activated protein kinase and phosphatidylinositol 3-kinase activities have opposite effects on human neutrophil apoptosis. FASEB J. 16, 129–131.

Alvarado-Kristensson, M., Rodriguez, M.J., Silio, V., Valpuesta, J.M., Carrera, A. C., 2009. SADB phosphorylation of gamma-tubulin regulates centrosome duplication. Nat. Cell Biol. 11, 1081–1092.

Batzenschlager, M., Masoud, K., Janski, N., Houlne, G., Herzog, E., Evrard, J.L., Baumberger, N., Erhardt, M., Nomine, Y., Kieffer, B., et al., 2013. The GIP gamma-tubulin complex-associated proteins are involved in nuclear architecture in Arabidopsis thaliana. Front. Plant Sci. 4, 480.

Brown, M.B., Miller, J.N., Seare, N.J., 1995. An investigation of the use of nile red as a long-wavelength fluorescent probe for the study of alpha 1-acid glycoprotein-drug interactions. J. Pharm. Biomed. Anal. 13, 1011–1017.

Collas, P., 1999. Sequential PKC- and Cdc2-mediated phosphorylation events elicit zebrafish nuclear envelope disassembly. J. Cell Sci. 112 (Pt 6), 977–987.

Cox, L.S., Leno, G.H., 1990. Extracts from eggs and oocytes of Xenopus laevis differ in their capacities for nuclear assembly and DNA replication. J. Cell Sci. 97 (Pt 1), 177–184.

Dechat, T., Adam, S.A., Taimen, P., Shimi, T., Goldman, R.D., 2010. Nuclear lamins. Cold Spring Harb. Perspect. Biol. 2, a000547.

Dent, J.A., Polson, A.G., Klymkowsky, M.W., 1989. A whole-mount immunocytochemical analysis of the expression of the intermediate filament protein vimentin in Xenopus. Development 105, 61–74.

Draberova, E., D'Agostino, L., Caracciolo, V., Sladkova, V., Sulimenko, T., Sulimenko, V., Sobol, M., Maounis, N.F., Tzelepis, E., Mahera, E., et al., 2015. Overexpression and Nucleolar Localization of gamma-Tubulin Small Complex Proteins GCP2 and GCP3 in Glioblastoma. J. Neuropathol. Exp. Neurol. 74, 723–742.

Ehlen, A., Rossello, C.A., von Stedingk, K., Hoog, G., Nilsson, E., Pettersson, H. M., Jirstrom, K., Alvarado-Kristensson, M., 2012. Tumors with nonfunctional retinoblastoma protein are killed by reduced gamma-tubulin levels. J. Biol. Chem. 287, 17241–17247.

Eklund, G., Lang, S., Glindre, J., Ehlen, A., Alvarado-Kristensson, M., 2014. The Nuclear Localization of gamma-Tubulin Is Regulated by SadB-mediated Phosphorylation. J. Biol. Chem. 289, 21360–21373.

Felix, M.A., Antony, C., Wright, M., Maro, B., 1994. Centrosome assembly in vitro: role of gamma-tubulin recruitment in Xenopus sperm aster formation. J. Cell Biol. 124, 19–31.

 http://dx.doi.org/10.1016/j.heliyon.2016.e00166

Hoog, G., Zarrizi, R., von Stedingk, K., Jonsson, K., Alvarado-Kristensson, M., 2011. Nuclear localization of gamma-tubulin affects E2F transcriptional activity and S-phase progression. FASEB J. 25, 3815–3827.

Horejsi, B., Vinopal, S., Sladkova, V., Draberova, E., Sulimenko, V., Sulimenko, T., Vosecka, V., Philimonenko, A., Hozak, P., Katsetos, C.D., et al., 2012. Nuclear gamma-tubulin associates with nucleoli and interacts with tumor suppressor protein C53. J. Cell. Physiol. 227, 367–382.

Kollman, J.M., Merdes, A., Mourey, L., Agard, D.A., 2011. Microtubule nucleation by gamma-tubulin complexes. Nat. Rev. Mol. Cell Biol. 12, 709–721.

Leno, G.H., Laskey, R.A., 1991. The nuclear membrane determines the timing of DNA replication in Xenopus egg extracts. J. Cell Biol. 112, 557–566.

Lesca, C., Germanier, M., Raynaud-Messina, B., Pichereaux, C., Etievant, C., Emond, S., Burlet-Schiltz, O., Monsarrat, B., Wright, M., Defais, M., 2005. DNA damage induce gamma-tubulin-RAD51 nuclear complexes in mammalian cells. Oncogene 24, 5165–5172.

Lindstrom, L., Villoutreix, B.O., Lehn, S., Hellsten, R., Nilsson, E., Crneta, E., Olsson, R., Alvarado-Kristensson, M., 2015. Therapeutic Targeting of Nuclear gamma-Tubulin in RB1-Negative Tumors. Mol. Cancer Res. 13, 1073–1082.

Lohka, M.J., Masui, Y., 1983. The germinal vesicle material required for sperm pronuclear formation is located in the soluble fraction of egg cytoplasm. Exp. Cell Res. 148, 481–491.

Lopez-Soler, R.I., Moir, R.D., Spann, T.P., Stick, R., Goldman, R.D., 2001. A role for nuclear lamins in nuclear envelope assembly. J Cell Biol. 154, 61–70.

Losada, A., Hirano, M., Hirano, T., 1998. Identification of Xenopus SMC protein complexes required for sister chromatid cohesion. Genes Dev. 12, 1986–1997.

Lourim, D., Kempf, A., Krohne, G., 1996. Characterization and quantitation of three B-type lamins in Xenopus oocytes and eggs: increase of lamin LI protein synthesis during meiotic maturation. J. Cell Sci. 109 (Pt 7), 1775–1785.

Lu, Z.H., Sittman, D.B., Brown, D.T., Munshi, R., Leno, G.H., 1997. Histone H1 modulates DNA replication through multiple pathways in Xenopus egg extract. J. Cell Sci. 110 (Pt 21), 2745–2758.

Ma, L., Tsai, M.Y., Wang, S., Lu, B., Chen, R., Iii, J.R., Zhu, X., Zheng, Y., 2009. Requirement for Nudel and dynein for assembly of the lamin B spindle matrix. Nat. Cell. Biol. 11, 247–256.

Martin, O.C., Gunawardane, R.N., Iwamatsu, A., Zheng, Y., 1998. Xgrip109: a gamma tubulin-associated protein with an essential role in gamma tubulin ring

 http://dx.doi.org/10.1016/j.heliyon.2016.e00166

complex (gammaTuRC) assembly and centrosome function. J. Cell Biol. 141, 675–687.

Mendez, J., Stillman, B., 2000. Chromatin association of human origin recognition complex, cdc6, and minichromosome maintenance proteins during the cell cycle: assembly of prereplication complexes in late mitosis. Mol. Cell. Biol. 20, 8602–8612.

Murray, A.W., 1991. Cell cycle extracts. Methods Cell Biol. 36, 581–605.

O'Brien, L.L., Wiese, C., 2006. TPX2 is required for postmitotic nuclear assembly in cell-free Xenopus laevis egg extracts. J. Cell Biol. 173, 685–694.

Peter, M., Nakagawa, J., Doree, M., Labbe, J.C., Nigg, E.A., 1990. In vitro disassembly of the nuclear lamina and M phase-specific phosphorylation of lamins by cdc2 kinase. Cell 61, 591–602.

Thompson, L.J., Bollen, M., Fields, A.P., 1997. Identification of protein phosphatase 1 as a mitotic lamin phosphatase. J. Biol. Chem. 272, 29693–29697.

Tsai, M.Y., Wang, S., Heidinger, J.M., Shumaker, D.K., Adam, S.A., Goldman, R. D., Zheng, Y., 2006. A mitotic lamin B matrix induced by RanGTP required for spindle assembly. Science 311, 1887–1893.

Xue, J.Z., Woo, E.M., Postow, L., Chait, B.T., Funabiki, H., 2013. Chromatin-bound Xenopus Dppa2 shapes the nucleus by locally inhibiting microtubule assembly. Dev. Cell 27, 47–59.

Yokoyama, H., Koch, B., Walczak, R., Ciray-Duygu, F., Gonzalez-Sanchez, J.C., Devos, D.P., Mattaj, I.W., Gruss, O.J., 2014. The nucleoporin MEL-28 promotes RanGTP-dependent gamma-tubulin recruitment and microtubule nucleation in mitotic spindle formation. Nat. Commun. 5, 3270.

 http://dx.doi.org/10.1016/j.heliyon.2016.e00166